Co-emission of volcanic sulfur and halogens amplifies volcanic effective radiative forcing

John Staunton-Sykes[*1], Thomas J. Aubry[2,4], Youngsub M. Shin[1], James Weber[1], Lauren R. Marshall[1], Nathan Luke Abraham[1,3], Alex Archibald[1,3], Anja Schmidt[1,2]

[1]*Centre for Atmospheric Science, Department of Chemistry, University of Cambridge, Cambridge, UK*

[2]*Department of Geography, University of Cambridge, Cambridge, UK*

[3]*National Centre for Atmospheric Science, UK*

[4]*Sidney Sussex College, Cambridge, UK*

Correspondence to: J. Staunton-Sykes (email:jjas3@cam.ac.uk)

Abstract

The evolution of volcanic sulfur and the resulting radiative forcing following explosive volcanic eruptions is well understood. Petrological evidence suggests that significant amounts of halogens may be co-emitted alongside sulfur in some explosive volcanic eruptions, and satellite evidence indicates that detectable amounts of these halogens may reach the stratosphere. In this study, we utilise an aerosol-chemistry-climate model to simulate stratospheric volcanic eruption emission scenarios of two sizes, both with and without co-emission of volcanic halogens, in order to understand how co-emitted halogens may alter the life cycle of volcanic sulfur, stratospheric chemistry and the resulting radiative forcing. We simulate a large (10 Tg of SO_2) and very large (56 Tg of SO_2) sulfur-only eruption scenario and a corresponding large (10 Tg SO_2, 1.5 Tg HCl, 0.0086 Tg HBr) and very large (56 Tg SO_2, 15 Tg HCl, 0.086 Tg HBr) co-emission eruption scenario. The eruption scenarios simulated in this work are hypothetical, but they are comparable to Volcanic Explosivity Index (VEI) 6 (e.g. 1991 Mt. Pinatubo) and VEI 7 (e.g. 1257 Mt. Samalas) eruptions, representing 1 in 50-100 year and 1 in 500-1000 year events respectively, with plausible amounts of co-emitted halogens based on satellite observations and volcanic plume modelling.

We show that co-emission of volcanic halogens and sulfur into the stratosphere increases the volcanic effective radiative forcing (ERF) by 24% and 30% in large and very large co-emission scenarios compared to sulfur-only emission. This is caused by an increase in both the forcing from volcanic aerosol-radiation interactions (ERF_{ari}) and composition of the stratosphere ($ERF_{clear,clean}$). Volcanic halogens catalyse the destruction of stratospheric ozone, which results in significant stratospheric cooling, offsetting the aerosol heating simulated in sulfur-only scenarios and resulting in net stratospheric cooling. The ozone induced stratospheric cooling prevents aerosol self-lofting and keeps the volcanic aerosol lower in the stratosphere with a shorter lifetime, resulting in reduced growth due to condensation and coagulation and smaller peak global-mean effective radius compared to sulfur-only simulations. The smaller effective radius found in both co-emission scenarios is closer to the peak scattering efficiency radius of sulfate aerosol, thus, co-emission of halogens results in larger peak global-mean ERF_{ari} (6% and 8%). Co-emission of volcanic halogens results in significant stratospheric ozone, methane and water vapour

Deleted: Anja Schmidt[1,2],

Deleted: In this study, we confront an aerosol-chemistry-climate model with four stratospheric volcanic eruption emission scenarios (56 Tg SO_2 ± 15 Tg HCl & 0.086 Tg HBr and 10 Tg SO_2 ± 1.5 Tg HCl & 0.0086 Tg HBr) in order to understand how co-emitted halogens may alter the life cycle of volcanic sulfur, stratospheric chemistry and the resulting radiative forcing. The eruption sizes simulated in this work are hypothetical Volcanic Explosivity Index (VEI) 7 (e.g. 1257 Mt. Samalas) and VEI 6 (e.g. 1991 Mt. Pinatubo) eruptions, representing 1 in 500-1000 year and 1 in 50-100 year events respectively, with plausible amounts of co-emitted halogens based on satellite observations and volcanic plume modelling.

Deleted: ERF

Deleted: (1.5 - 3 K); counteracting the typical

Deleted:

Deleted: stratospheric radiative

Deleted: from

Deleted: volcanic sulfate aerosol

reductions, resulting in significant increases in peak global-mean $ERF_{clear,clean}$ (>100%), predominantly due to ozone loss. The dramatic global-mean ozone depletion simulated in large (22%) and very large (57%) co-emission scenarios would result in very high levels of UV exposure on the Earth's surface, with important implications for society and the biosphere. This work shows for the first time that co-emission of plausible amounts of volcanic halogens can amplify the volcanic ERF in simulations of explosive eruptions; highlighting the need to include volcanic halogen emissions when simulating the climate impacts of past or future eruptions, and to maintain space-borne observations of stratospheric compounds to better constrain the stratospheric injection estimates of volcanic eruptions.

Deleted: both

Deleted: simulations (22%, 57%)

Deleted: need

Deleted: fluxes

Deleted: providing motivation to better quantify the degassing budgets and stratospheric injection estimates for volcanic eruptions.

1 Introduction

Sulfur gases emitted into the atmosphere by volcanic eruptions have a strong direct climate impact through the formation of sulfuric acid aerosol, which reflect incoming sunlight and cool the Earth's surface (Robock, 2000). Volcanic aerosols also have the potential to alter the chemistry of the stratosphere, including ozone with significant impacts on both longwave and shortwave radiative fluxes. Ozone is impacted dynamically by stratospheric circulation changes induced by aerosol heating, and chemically by changes to ozone catalytic loss cycles. Aerosol heating in the tropics increases the vertical ascent transporting ozone to higher altitudes and latitudes, resulting in an ozone decrease in the tropics and an increase at high latitudes (Kinne, Toon and Prather, 1992). The addition of large amounts of volcanic aerosols increases the surface area of the stratosphere on which heterogeneous reactions can take place (Solomon, 1999). Heterogeneous reactions in the stratosphere drive changes in the partitioning of NO_x, ClO_x, BrO_x and HO_x species between reservoir and active forms. Unlike polar stratospheric clouds (PSCs), which only occur in the extremely cold temperatures inside the winter polar vortex, volcanic aerosols provide surfaces for heterogeneous reactions at all latitudes and at all times of the year. N_2O_5 reacts with water vapour on the surfaces of these volcanic aerosols to form HNO_3, effectively sequestering reactive NO_x species into a long-lived reservoir and limiting the availability of NO_x radicals to take part in catalytic reactions which deplete stratospheric ozone, reducing the chemical destruction of ozone (Crutzen, 1970; Johnston, 1971). In contrast, these reactions liberate reactive ClO_x and BrO_x species from their long-lived reservoirs, increasing the chemical destruction of ozone (Solomon *et al.*, 1996; Solomon, 1999; Aquila *et al.*, 2013).

The net chemical impact of volcanic sulfate aerosol loading on stratospheric ozone is dependent on the stratospheric halogen loading (e.g., Timmreck, 2012). A large volcanic eruption in low-halogen atmospheric conditions, such as a preindustrial or future atmosphere, is expected to result in a net stratospheric ozone increase (Langematz et al., 2018), however, when the halogen loading of the stratosphere is high, an eruption will lead to a net stratospheric ozone decrease (e.g. Tie & Brasseur, 1995). High-halogen loading may arise from anthropogenic or natural emissions. Petrological data suggest that volcanic eruptions in some geological settings may also release substantial amounts of halogen gases into the atmosphere (Kutterolf *et al.*, 2013, 2015; Krüger, Kutterolf and Hansteen, 2015). Petrological analysis of the 1257 Mt. Samalas eruption suggests as much as 227 Tg of hydrogen chloride (HCl) and 1.3 Tg of hydrogen bromide (HBr) could have been emitted into the atmosphere alongside 158 Tg of sulfur dioxide (SO_2) (Vidal *et al.*, 2016). The portion of the halogens erupted at the vent that reach the stratosphere (hereafter halogen injection efficiency) is not well constrained and has been the subject of debate in the community for decades. Halogens are soluble (especially HCl) and may be scavenged

by water, ice hydrometeors and ash in the volcanic plume (Halmer, Schmincke and Graf, 2002). Despite efficient scavenging, direct stratospheric injection of volcanic halogens is predicted by theory, and sophisticated plume models suggest that between 10% and 20% of the HCl emitted at the vent of large explosive eruptions could reach the stratosphere (Textor *et al.*, 2003).

Aircraft measurements following the 2000 Mt. Hekla eruption in Iceland showed that 75% of the HCl emitted at the vent entered the lower stratosphere and was still present 35 hours after the eruption suggesting that little scrubbing took place in the tropospheric eruption column (Hunton *et al.*, 2005; Rose *et al.*, 2006). Read *et al.* (2009) used retrievals from the Microwave Limb Sounder (MLS) to show that SO_2 and HCl was injected directly into the lower stratosphere during the 2004 Manam, 2007 Anatahan, 2008 Soufriere Hills, 2008 Okmok, 2008 Kasatochi, 2009 Redoubt, and 2009 Sarychev eruptions. Using retrievals from MLS, Prata *et al.* (2007) reported HCl at ~20 km in the volcanic plume of 2006 Soufriere Hills eruption plume, with stratospheric HCl:SO_2 gas ratios <0.1. Carn *et al.*, (2016) reported MLS stratospheric HCl:SO_2 gas ratios of 0.01–0.03 (relative mixing ratios) for 14 small eruptions in the period between 2005 to 2014. Limitations with the field of view and spatial sampling of MLS mean these observed ratios are likely an underestimate (Carn *et al.*, 2016).

Petrological analysis in Bacon *et al.* (1992) suggested that the considerably larger, Volcanic Explosivity Index (VEI) 7, 7.6 kya eruption of Mt. Mazama degassed ~100 Tg of Cl, and the ice core record of the same eruption suggested 8.1 Tg Cl and 57.5 Tg SO_2 was injected into the stratosphere with a halogen injection efficiency of 8.1% and a stratospheric HCl:SO_2 molar ratio of ~0.3 (Zdanowicz *et al.*, 1999). The two largest eruptions in the satellite era, 1982 El Chichón and 1991 Mt. Pinatubo, highlight the variability in stratospheric halogen injection following explosive volcanic eruptions. Both eruptions released relatively small amounts of halogens, 1.8 Tg (Varekamp *et al.*, 1984) and 4.5 Tg of chlorine respectively with HCl:SO_2 molar ratios of ~0.4 (Mankin *et al.*, 1992). Spectroscopic measurements of the El Chichón stratospheric eruption plume indicated an HCl increase of 40% compared to measurements taken prior to the eruption, with a stratospheric injection of >0.04 Tg of HCl and a halogen injection efficiency of at least 2.5% (Mankin and Coffey, 1984; Woods *et al.*, 1985). Woods et al. (1985) measured NaCl salt particles in the lower stratospheric eruption cloud of El Chichón derived from the chlorine-rich magma. They hypothesised that the rapid ascent of large Plinian eruption phases led to the formation of ice-bearing crystals and salt particles, which would lower the halogen scrubbing efficiency and preserve the halogens for stratospheric release. In the stratosphere, these salt particles may react with volcanic sulfuric acid leading to the formation of secondary HCl. In contrast, despite emitting more Cl into the atmosphere than El Chichón, observations following 1991 Mt. Pinatubo showed minimal stratospheric halogen injection as the halogens were more efficiently scavenged in the eruption cloud (Wallace and Livingston, 1992). The Pinatubo eruption occurred at the same time and location as a typhoon in the Philippines, and it is thought these very wet tropospheric conditions led to the effective wash out of halogens (McCormick *et al.*, 1995; Gerlach *et al.*, 1996; Self S *et al.*, 1996).

Overall, current datasets show that the stratospheric injection of volcanic halogens is highly variable and depends on both the total mass of halogens released at the vent and the degree of scavenging, determined by the geochemistry of the volcano and the prevailing atmospheric conditions during the eruption, particularly the

Deleted: Moun

Deleted: s

Deleted: made in

Deleted: local

Deleted: ,

Deleted: (halite)

Deleted: o

Deleted: p

Deleted: halite

Deleted: halite

humidity. It is clear, however, that volcanic halogens are injected into the stratosphere after some volcanic eruptions, and research into how these volcanic halogens may alter the volcanic aerosol microphysics, stratospheric chemistry, and the volcanic forcing is still limited.

Lurton *et al.* (2018) simulated the 2009 Sarychev Peak eruption (0.9 Tg of SO_2) in CESM1(WACCM) (Community Earth-System Model, Whole Atmosphere Community Climate Model) and showed how inclusion of co-emitted halogens (27 Gg of HCl) resulted in a lengthening of the SO_2 lifetime, due to the further depletion of OH, and a corresponding delay in the formation of aerosols, giving better agreement between modelled and observed SO_2 burden and showing how co-emitted halogens could impact volcanic sulfur processing.

Tie and Brasseur (1995) utilised model calculations to show how background atmospheric chlorine loadings altered the ozone response to volcanic sulfur injections. In conditions typical of the pre-1980 period, the ozone column abundance was shown to increase after a large volcanic eruption. The increase in column abundance resulted from suppression of the NOx catalysed ozone loss cycle, driven by the sequestration of reactive nitrogen to its reservoir species via heterogeneous reactions on the surface of volcanic aerosol. The ozone response was shown to be independent of the magnitude of the eruption, as the heterogeneous conversion of active nitrogen to its reservoir was saturated. However, after 1980, higher background chlorine levels as a result of anthropogenic emissions of chlorofluorocarbons, meant that the ozone response became negative in winter at mid and high latitudes. The suppression of NOx catalysed ozone loss was counterbalanced by an increase in the ClOx catalysed ozone loss, resulting in a transition in the column ozone response. Unlike in pre-industrial conditions, the ozone response was dependent on the eruption size as the heterogeneous conversion of chlorine species from reservoir to reactive is not saturated. Since then, a number of studies have investigated the impact of volcanic halogens on stratospheric ozone. Cadoux *et al.* (2015) petrologically determined chlorine and bromine degassing budgets for the Bronze Age (~1600 BCE) Santorini eruption and, using a halogen injection efficiency of 2%, input 36 Tg S, 13.5 Tg Cl and 0.02 Tg Br uniformly between the tropopause and 35 km in a pre-industrial background state within a 2D chemical transport model (CTM). They simulated ozone depletion lasting a decade with a peak global-mean of 20-90% over the NH. The molar ratio of HCl and SO_2 injected into the stratosphere ($HCl:SO_2$) in this study was 0.64, considerably larger than observations from MLS (<0.1) and ice core records of Mt. Manzana (<0.3). Klobas *et al.* (2017), also used a 2D CTM to study the impact that co-emission of volcanic halogens has on column ozone in contemporary and future background states. They simulated hypothetical Pinatubo sized eruptions with a $HCl:SO_2$ of ~0.14, and reported global ozone depletion lasting ~2-3 years with a peak of 20%. These CTM studies used prescribed wind fields and, as a result, do not include the important interactive feedbacks of radiation and dynamics which alter the transport of tracers and thus the composition of the atmosphere. Ming *et al.* (2020) simulated explosive tropical eruptions in a chemistry-climate model which consisted of the UK Met Office Unified Model (UM) together with the United Kingdom Chemistry and Aerosol (UKCA) scheme, including the interactive stratospheric aerosol model GLOMAP-mode (Mann *et al.*, 2010). They simulated 6 sets of experiments: low SO_2 (10 Tg) and high SO_2 (100 Tg) eruptions paired with no HCl, low HCl (0.02 Tg) and high HCl (2 Tg), and reported significant ozone depletion over both poles for at least four years in the high SO_2 and high HCl experiment. Brenna *et al.* (2019) used CESM1(WACCM) with prescribed volcanic aerosols and sea surface temperatures (SSTs) to simulate an average eruption of a Central American Volcanic Arc volcano in a

Deleted: The
Deleted: (WACCM
Deleted: allowed
Deleted: with
Deleted: data
Deleted: . Co-emission of halogens resulted in a lengthening of the SO_2 lifetime due to the further depletion of OH and a corresponding delay in the formation of aerosols with good agreement to in situ stratospheric measurements,
Deleted: ing
Deleted: .
Deleted: In conditions typical of the pre-1980 period, the ozone column abundance was shown to increase after a large volcanic eruption with the response being independent of the magnitude of the eruption. However, after 1980, higher background chlorine levels as a result of anthropogenic emissions of chlorofluorocarbons, meant that the ozone response became negative in winter at mid and high latitudes, with the magnitude of depletion increasing with eruption size.
Deleted: prior
Deleted: ,
Deleted: of
Deleted: The stratospheric injection $HCl:SO_2$ molar ratio of
Deleted: is
Deleted: Moun
Deleted: ,
Deleted: stratospheric injection
Deleted: mixing ratio
Deleted: ,
Deleted: the
Deleted:
Deleted: UM-UKCA
Deleted: and
Deleted: found
Deleted: that a volcanic halogen emission of 0.02 Tg ($HCl:SO_2$ = 0.04) into a pre-industrial background state had little impact on column ozone but 2 Tg ($HCl:SO_2$ = 0.4) showed significant and prolonged ozone depletion above both poles.

pre-industrial background state, with a 10% halogen injection efficiency (2.5 Tg Cl, 9.5 Gg Br). They found ozone depletion of up to 20% globally for 10 years, with ozone hole conditions over the tropics and Antarctica. Consequently, UV radiation increases of >80% were simulated in the tropics, averaging to >40% for 2 years.

These studies did not, however, investigate how volcanic halogens may interact with the sulfur aerosol life cycle and interact to modulate volcanic forcing. Brenna *et al.* (2020) used Community Earth System Model 2 (WACCM6) to investigate the coupling and feedback between volcanic aerosol, chemistry, radiation and climate pre-industrial background state. They investigate the combined effect of the sulfur (523 Tg S) and halogens (120 Tg Cl, 0.2 Tg Br) emissions of the Los Chocoyos supereruption, assuming a 10% halogen injection efficiency resulting in a stratospheric HCl:SO_2 molar ratio ~0.4, on volcanic gases, ozone and surface UV. Compared to simulations with sulfur-only injections, they simulate a lower peak sulfate burden attributed to the delay in SO_2 oxidation but with the same total sulfur lifetime and aerosol effective radius. Thus, the co-emission of halogens results in a smaller radiative forcing, 20% lower compared to sulfur-only. Wade *et al.* (2020) compared HadGEM3-ES (Earth System configuration of the Hadley Centre Global Environment Model version 3) simulations of the 1257 Mt. Samalas eruption, utilising the halogen degassing estimates from Vidal *et al*. (2016) and stratospheric halogen injection efficiencies of 20% and 1%, with the available surface temperature proxies. Their results suggest it is unlikely that 20% of degassed halogens reached the stratosphere, however smaller fractions gave good agreement with multi-proxy surface temperature records.

The aim of this study is to simulate hypothetical large and very-large sized eruptions, both with and without halogens in a coupled chemistry-aerosol model and investigate how the co-emission of volcanic sulfur and halogens alters the evolution of volcanic aerosol, ozone, stratospheric composition, and the consequential radiative forcing and UV flux.

2 Data and Methods

2.1 Model Description

This study uses UKESM-AMIP, the atmosphere-only configuration of the UK Earth System Model UKESM1.0 (Sellar *et al.*, 2019) including coupled aerosol-chemistry-climate components consisting of the United Kingdom Chemistry and Aerosol (UKCA) module together with the UK Met Office Unified Model (UM). The UKCA module is run at UM version 11.2 with the combined stratosphere and troposphere chemistry (StratTrop) scheme (Archibald *et al.*, 2020). The model is free-running in the atmosphere, forced by sea ice and sea surface temperature surface boundary conditions, similar to the set up used in the UK Earth system model (UKESM1) Atmospheric Model Intercomparison Project (AMIP) simulations submitted to the Coupled Model Intercomparison Project Phase 6 (CMIP6) (Sellar *et al.*, 2019, 2020). The resolution was 1.875° longitude by 1.25° latitude with 85 vertical levels extending from the surface to 85 km. The dynamics of the stratosphere have previously been shown to be well represented in this model, and it has an internally generated Quasi-Biennial Oscillation QBO (Osprey *et al.*, 2013) The model includes the fully interactive stratospheric GLOMAP-mode aerosol scheme which simulates microphysical processes including the formation, growth, transport and loss of

Deleted: and

Deleted: ¶
¶
Very recently

Deleted: confront a

Deleted: with

Deleted: hypothetical VEI 6 and VEI 7 sized eruptions, both with and without halogens,

Deleted: utilises

Deleted: the

Deleted: model

Deleted: T

Deleted: (sea ice and sea surface temperatures),

aerosol (Dhomse *et al.*, 2014). GLOMAP-mode also calculates aerosol optical properties online which are used to calculate direct and indirect radiative effects (Mulcahy *et al.*, 2020).

In UKCA, stratospheric ozone concentrations are determined by sets of photochemical reactions as well as ozone destroying catalytic cycles involving chlorine, bromine, nitrogen, and hydrogen radical species (Archibald *et al.*, 2020). Photolysis reactions in UKCA utilise rates calculated from a combination of the FAST-JX scheme and look-up tables (Telford *et al.*, 2013). Ozone depleting radical species are produced by the photolysis of halogen containing compounds reacting on the surface of stratospheric aerosols, including hydrochloric acid (HCl), chlorine nitrate ($ClONO_2$), hydrogen bromide (HBr), and bromine nitrate ($BrONO_2$). Heterogeneous reactions in the presence of polar stratospheric clouds (PSCs) in the polar lower stratosphere or in the presence of sulfate aerosol following explosive volcanic eruptions are also important for stratospheric ozone concentrations. Eight additional heterogeneous reactions involving chlorine and bromine species were added as described in Ming *et al*. (2020), with the main change being the explicit treatment of the reactions of four additional chemical species: Cl_2, Br_2, $ClNO_2$, and $BrNO_2$ which are photolysed to produce Cl and Br radicals.

Volcanic effective radiative forcings (hereafter *ERF)* are calculated as differences (Δ) in the net top of atmosphere (TOA) radiative fluxes (F) between perturbed and control climatologies, as follows:

$$ERF = \Delta F \qquad Eq.\,1$$

Volcanic ERF is decomposed as described in (Schmidt *et al.*, 2018) and (Ghan, 2013), as follows:

$$ERF = \Delta(F - F_{clean}) + \Delta\left(F_{clean} - F_{clear,clean}\right) + \Delta F_{clear,clean} \qquad Eq.\,2$$

$$= ERF_{ari} + ERF_{aci} + ERF_{clear,clean} \qquad Eq.\,3$$

This decomposition is enabled by implementing extra calls to the radiation scheme as recommended by Ghan (2013) to obtain F_{clean} and $F_{clear,clean}$. Where F_{clean} denotes a radiation flux diagnostic calculation without aerosol-radiation interactions but including aerosol-cloud interactions through microphysics. $F_{clear,clean}$ denotes a radiation flux diagnostic calculation that ignores both aerosol and cloud-radiation interactions. Thus, $F - F_{clean}$, determines the impact of all aerosols and $\Delta(F - F_{clean})$ is an estimate of the forcing from volcanic aerosol-radiation interactions (ERF_{ari}). The second term $\Delta(F_{clean} - F_{clean,clear})$ represents the difference in the clean-sky cloud radiative forcing, and is an estimate of the aerosol-cloud interactions (ERF_{aci}) due to volcanic emissions. The third term, $ERF_{clear,clean}$ accounts for changes not directly due to aerosol or cloud interactions, largely the result of changes in surface albedo and atmospheric composition.

2.2 Experimental Design

We utilise atmosphere-only, time-slice experiments whereby the SST, sea ice fraction and depth, surface emissions and lower boundary conditions are prescribed using climatologies calculated using data from the fully coupled UKESM1.0 historical runs produced for CMIP6 (Eyring *et al.*, 2016) and averaged over the years 1990 to 2000. By averaging over the decade the atmosphere-only simulations are forced with boundary conditions typical of the recent historical period but not a specific date within that decade. The fully coupled transient

Deleted: simulations

Deleted: In this study, we fix surface temperature and sea-ice fields meaning that surface albedo is expected to be unchanged and any $F_{clear,clean}$ changes are the result of atmospheric compositional changes.

Deleted: We utilise atmosphere-only, time-slice experiments whereby the initial sea surface temperature, sea ice fraction and forcing agents are prescribed climatologies with values taken from fully coupled UKESM1.0 historical runs produced for CMIP6 (Eyring et al. 2016) and averaged over the years 1990 - 2000. The 1990s, and thus these timeslices, were characterised by high background halogen levels due to anthropogenic emissions of CFCs throughout the preceding decade. A control simulation was run with a 15 year spin up followed by a further 20 years. The effect of explosive volcanic eruptions was investigated by running a series of 10 year volcanic perturbations spun off from 6 different years in the control run to represent the variability in QBO states. Changes are plotted as the difference between the average of the 6 ensembles and the climatology derived from the 20 year control run, cumulative forcings are calculated as the sum of the forcing over the full 10 year simulation duration. The volcanic emissions are prescribed by direct injection of SO_2, HCl and HBr into the stratosphere with a Gaussian plume vertical distribution centred on 21 km, lasting for 24 hours on July 1st. The gases were injected in the tropics (5°S latitude and 0° longitude) to represent a typical tropical explosive eruption (Newhall et al., 2017). ¶
¶

Deleted: sea surface temperature

simulations had internally generated El Nino and La Nina cycles, however, averaging the SSTs over the 1990 to 2000 period resulted in a permanent neutral signal in the SST pattern (see Figure S1). The 1990s, and thus these timeslices, were characterised by high background halogen levels due to anthropogenic emissions of CFCs throughout the preceding decade. The impacts of very short lived Bromine species are accounted for by adding a fixed contribution of 5 pptv into the CH3Br surface concentration.

A control simulation was initialised from the January 1995 initialisation file taken from the UKESM1.0 historical scenario which was run as part of CMIP6 (Eyring *et al.*, 2016). The model was allowed to spin up for 15 years and the control was run for a further 20 years. The effect of explosive volcanic eruptions was investigated by running a series of 10-year volcanic perturbation simulations spun off from 6 different years in the control run to represent the variability in QBO states. Changes are plotted as the difference between the average of the 6 ensembles and a climatology derived from the 20-year control run, cumulative forcings are calculated as the time-integrated forcing across the Earth's surface and represent the total energy loss (J) as a result of the volcanic eruption.

The volcanic emissions are prescribed by direct injection of SO_2, HCl and HBr into the stratosphere with a Gaussian vertical distribution centred on 21 km and a width of 2.1 km (10% of the height), lasting for 24 hours on July 1st. An injection altitude of 21 km was chosen as, allowing for lofting, this results in a volcanic plume altitude consistent with recent historical eruptions from the satellite era (Guo *et al.*, 2004). The gases were injected in the tropics (5ºS latitude and 0º longitude) to represent a typical tropical explosive eruption (Newhall *et al.*, 2018).

Since historical stratospheric volcanic SO_2 fluxes are variable and the volcanic flux of HCl and HBr into the stratosphere remains uncertain, we developed a simulation matrix that spans a range of possible explosive volcanic emissions. The four sets of experiments have one large SO_2 (10 Tg), and one very-large SO_2 (56 Tg) emission scenario both with (HAL10 and HAL56) and without halogens (SULF10 and SULF56), as shown in Table 1. These eruption sizes (10 and 56 Tg SO_2) are hypothetical, but they are comparable to a VEI 6 (e.g. 1991 Mt. Pinatubo) and VEI 7 (e.g. 1257 Mt. Samalas) eruption, representing 1 in 50-100 year and 1 in 500-1000 year events respectively (Newhall *et al.*, 2018). VEI is used here to provide context of the recurrence rates but is not used as an index representative of climate impact. HAL56 utilises the 1257 Mt. Samalas HCl and HBr emission estimates from Vidal *et al.* (2016) and assumes a conservative ~5% stratospheric halogen injection efficiency, less than the 10-20% predicted by plume modelling in Textor *et al.* (2013) and closer to the observed efficiency following El Chichón (>2.5%) and in the ice core record of Mt. Mazama (8%), as well as the fraction supported by Wade *et al.* (2020). HAL10 has a SO_2 injection similar to that found to reproduce the spatial and temporal evolution of stratospheric aerosol optical depth (SAOD) following 1991 Pinatubo (Mills *et al.*, 2016) and a 10 times smaller HCl and HBr flux than HAL56. This results in a HCl:SO_2 ratio of ~0.26 and ~0.47 in HAL10 and HAL56 respectively, similar to the estimated stratospheric injection ratio for Mt. Mazama (0.3) (Zdanowicz *et al.*, 1999) and the ratios used in Ming *et al.* (2020), and Brenna *et al.* (2020) but smaller than the ratio used in Cadoux *et al.* (2015).

Deleted: A 20-year control simulation was run with after 15 year spin up, initialised from the January 1995 initialisation file taken from the UKESM1.0 historical scenario which was run as part of CMIP6

Deleted: sum of the forcing over the full 10 year simulation duration

Deleted: plume

Deleted: high

Deleted: 56

Deleted: low

Deleted: 10

Deleted: 56

Deleted: 10

Deleted: 56

Deleted: 10

Deleted: 56

Deleted: 10

Deleted: similar in size

Moved down [2]: VEI 7 (e.g. 1257 Mt. Samalas) and

Moved (insertion) [2]

Deleted: and

Deleted: 0

Deleted: 0

Deleted: o

Deleted: This results in a HCl:SO_2 molar ratio of ~0.47, similar to the ratios simulated in Ming et al., 2020, and Brenna et al., 2020 and smaller than the ratio simulated in Cadoux et al., 2015. HAL10 has a SO_2 injection similar to 1991 Pinatubo and a 10 times smaller flux of HCl and HBr than HAL56, resulting in a HCl:SO_2 molar ratio of ~0.26, very close to the estimated stratospheric injection ratio for Mt. Mazama (0.3) (Zdanowicz et al., 1999).

Scenario	SO_2 (Tg)	HCl (Tg)	HBr (Tg)	HCl:SO_2
SULF56	56	-	-	-
HAL56	56	15	0.086	0.47
SULF10	10	-	-	-
HAL10	10	1.5	0.0086	0.26

Table 1 Showing the eruption masses of SO_2, HCl and HBr in Tg for the four sets of experiments.

Deleted: (molar ratio)

Deleted: Equivalent effective Stratospheric Chlorine (EESC) = [Cl] added to stratosphere+ 60 × [Br] added to stratosphere (Cadoux et al., 2015).

3 Results

3.1 Sulfur Microphysics and ERF_{ari}

Atmospheric burdens of volcanic sulfur species are summarized in Figure 1. As shown by Lurton *et al.* (2018), volcanic halogens deplete the hydroxyl radical (OH) via equation 4.

Deleted: found

Deleted: 1

$$HCl + OH \rightarrow Cl + H_2O \qquad \text{Eq. 4}$$

Deleted: 1

which limits the availability of OH for SO_2 oxidation, leading to slower destruction of volcanic SO_2 and an increase in SO_2 e-folding time of 21% and 40% in HAL10 and HAL56 compared to SULF10 and SULF56 respectively. As the rate of formation of sulfuric acid is decreased, we simulate a corresponding delay in the formation in sulfate aerosol and a reduction in the peak sulfate aerosol burden by 8% in both HAL10 and HAL56.

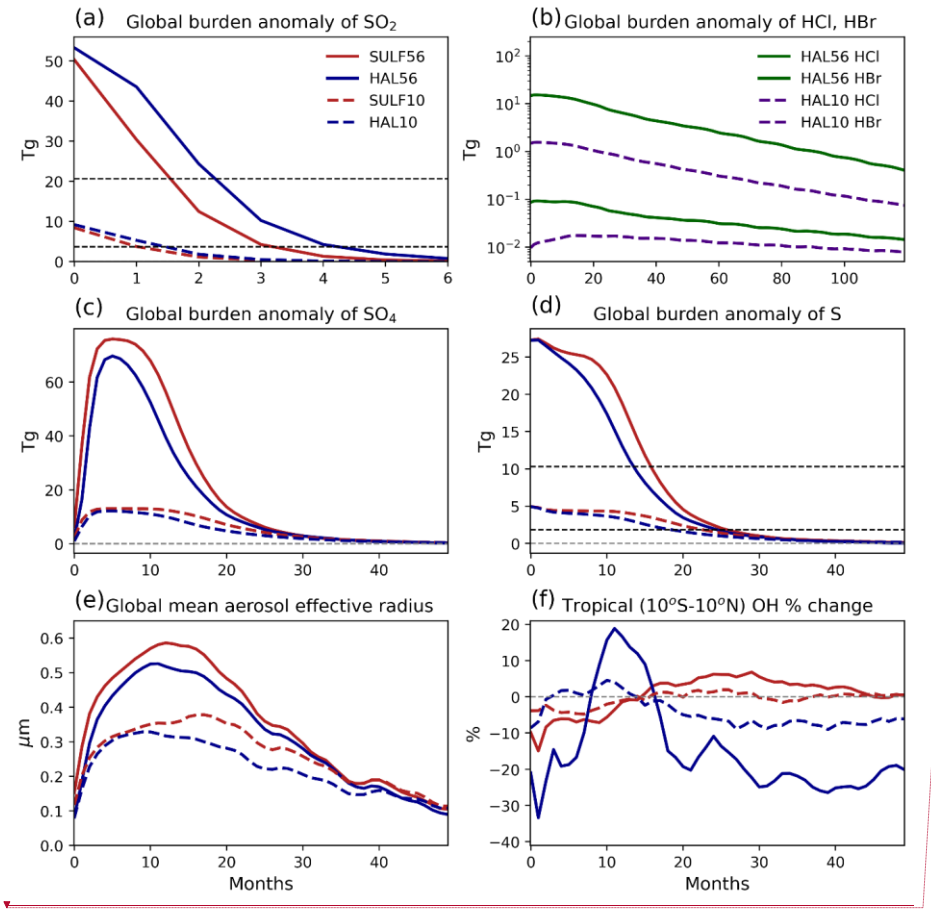

435

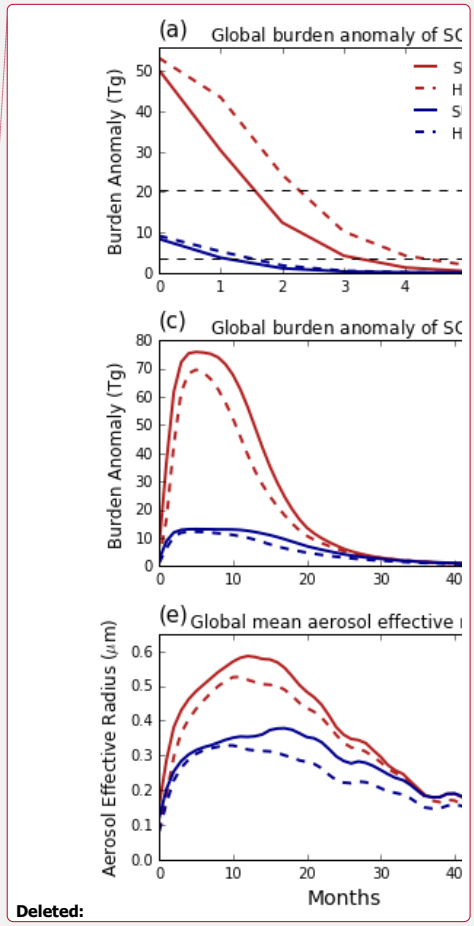

Deleted:

Figure 1 - Global evolution of sulfur, halogens and OH for the SULF56, HAL56, SULF10 and HAL10 simulations relative to the control climatology. **(a)** SO_2 burden anomalies. **(b)** HCl and HBr burden anomalies on log scale. **(c)** Sulfate aerosol burden anomalies. **(d)** Total sulfur burden anomalies. (e) Global-mean aerosol 440 effective radius, weighted by aerosol surface area density. **(f)** Tropical (20°N-20°S) stratospheric OH change (%). Dashed horizontal lines in (a) (b) and (d) represent the mass remaining after one e-folding lifetime. Note the different axis scales.

Deleted: 1/e

Despite the slower rate of SO_2 oxidation, the co-emission of halogens reduces the e-folding lifetime of the sulfur 445 burden to 17.3 and 11.7 months in HAL10 and HAL56, compared with 21.2 and 13.6 months in SULF10 and SULF56, a decrease of 18% and 14% respectively. This indicates that co-emission of halogens alters the rate at which sulfur is removed from the atmosphere. Significant differences in stratospheric temperature change are simulated between the sulfur-only and halogen simulations. In sulfur-only simulations, strong positive temperature anomalies of ~3 K due to sulfate aerosol absorption of infra-red radiation are simulated across the

tropical stratosphere (Figure 2). This aerosol heating increases the vertical ascent (Figure S2) and lofts volcanic aerosol to altitudes higher than the initial injection height in the model. By contrast, co-emission of volcanic halogens results in significant stratospheric ozone depletion of 22-57% (see section 3.2) and in turn this results in large negative temperature anomalies over most of the lower and middle stratosphere ~ -3 K (Figure 2). Ozone generates heat in the stratosphere by absorbing both incoming shortwave (SW) radiation from the Sun and by absorbing upwelling longwave (LW) radiation from the troposphere. Thus, decreasing stratospheric ozone results in stratospheric cooling, offsetting the volcanic aerosol heating and resulting in net stratospheric cooling. This stratospheric cooling decreases the vertical ascent in the tropics (Figure S2) and prevents volcanic sulfate aerosol being self-lofted in HAL10 and HAL56. The volcanic sulfate aerosol thus remains at significantly lower altitudes in HAL10 and HAL56 (~21-22km) compared with SULF10 and SULF56 (~24-25km) (Figure 2). Lower altitude aerosol remains in a faster region of the Brewer-Dobson Circulation (Figure S3) which results in faster transport to high-latitudes and removal from the stratosphere (Figure 1d).

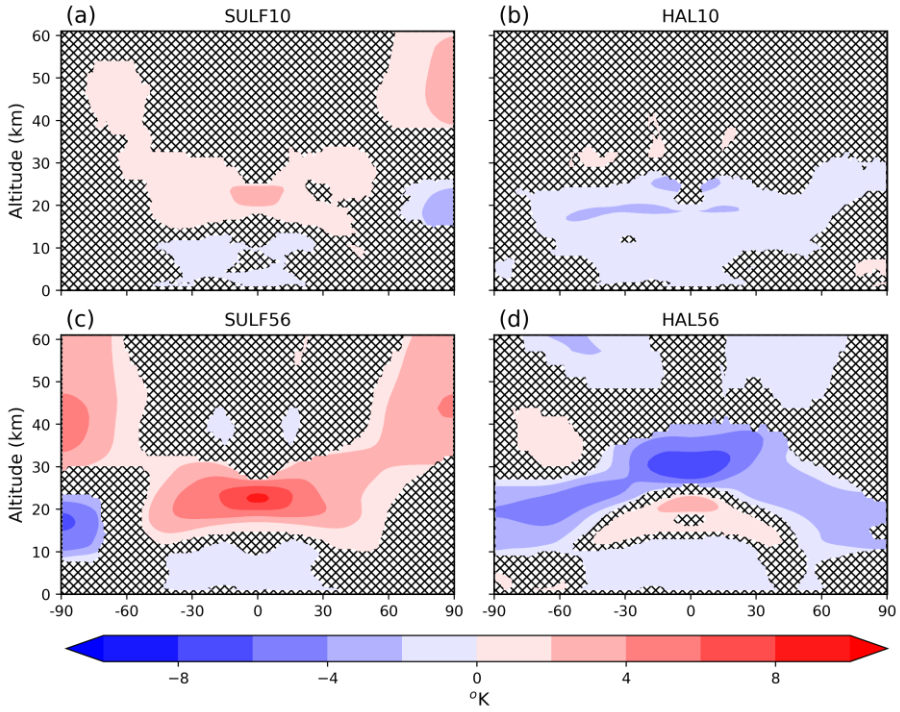

Deleted: s

Deleted: lower

Deleted: temperatures

Deleted: ; the effect of which is larger in magnitude than the aerosol heating and prevents

Deleted: branch

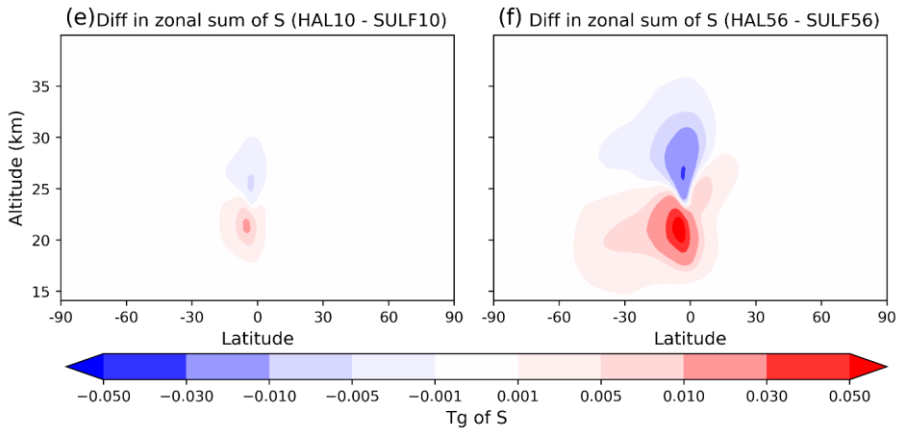

Figure 2 Zonal-mean temperature difference (°K) averaged over the first year post-eruption relative to the control climatology. **(a)** SULF56, **(b)** HAL56, **(c)** SULF10, **(d)** HAL10. Differences that are not significant at the 95% confidence interval according to a Mann–Whitney U test are indicated with stipples. Difference in zonal sum of total sulfur averaged over the first year post-eruption **(e)** HAL56 -SULF56, **(f)** HAL10 - SULF10.

The maximum global-mean aerosol effective radii (R_{eff}) was 0.38 μm and 0.59 μm in SULF10 and SULF56, respectively. The maximum global-mean R_{eff} simulated in SULF10 is similar to that derived from measurements following 1991 Pinatubo, with an estimate of 0.4 - 0.5 μm from balloon borne measurements (Deshler *et al.*, 1997) and 0.45 μm obtained from GLOSSAC satellite observations (GloSSAC, version 1.1; Thomason *et al.*, 2018). The shorter lifetime of sulfur in the atmosphere following HAL10 and HAL56 eruptions results in reduced aerosol growth and smaller R_{eff}. Peak global-mean R_{eff} is ~15% and ~10% smaller in HAL10 and HAL56 compared to their equivalent SULF simulations (Figure 1e). This aerosol growth stunting effect is a direct result of the shorter sulfur lifetime, rapid spreading and removal of aerosol. Volcanic sulfate aerosols grow through microphysical processes of condensation and coagulation (Kremser *et al.*, 2016). The faster removal of sulfate aerosol in HAL10 and HAL56 reduces the growth via condensation and coagulation and results in smaller peak global-mean aerosol R_{eff}. This theory is supported by Figure 3 which shows a scatter plot of 3-year global-mean aerosol effective radius as a function of the global sulfur burden e-folding lifetime for each individual ensemble member, with a significant correlation within both 10 Tg (r=0.88) and 56 Tg (r=0.95) eruption ensembles. The positive correlation between these two variables holds only for each eruption size scenario. To a first order, the aerosol R_{eff} is determined by the magnitude of the volcanic sulfur injection. The larger SO_2 injection in HAL56 and SULF56 ensemble simulations leads to larger-sized sulfate aerosols, faster sedimentation and shorter removal time compared to HAL10 and SULF10 ensemble simulations. However, when we fix the mass of sulfur injected and compare sulfur-only and co-emission scenarios, we find that transport has a second order effect. The faster removal of sulfate aerosol in HAL10 and HAL56 ensemble simulations leads to smaller-sized aerosol due to reduced opportunity for aerosol growth compared with SULF10 and SULF56 respectively.

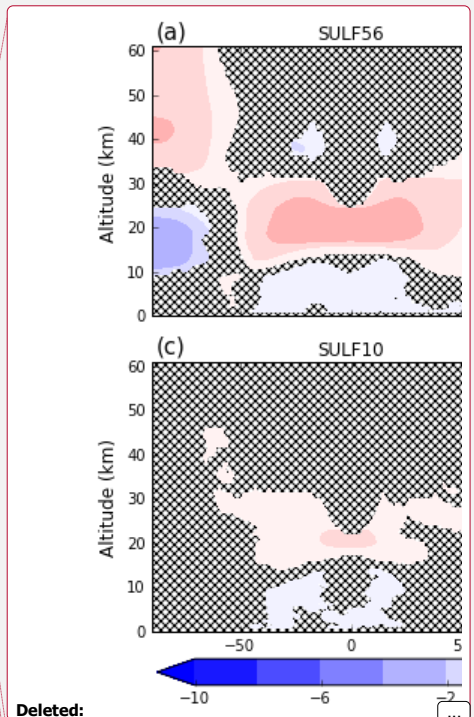

Deleted: ...
Deleted: ¶
Deleted:
Deleted: 3
Deleted: s
Deleted:
Moved (insertion) [1]
Deleted: Zonal d
Deleted: sulfur burden
Deleted:
Deleted: 2
Deleted: s
Deleted:
Moved up [1]: Differences that are not significant at the 95% confidence interval according to a Mann–Whitney U test are indicated with stipples.
Deleted: stunted
Deleted: aerosol effective radii (
Deleted: as seen by comparing Figures 3a and 3b.

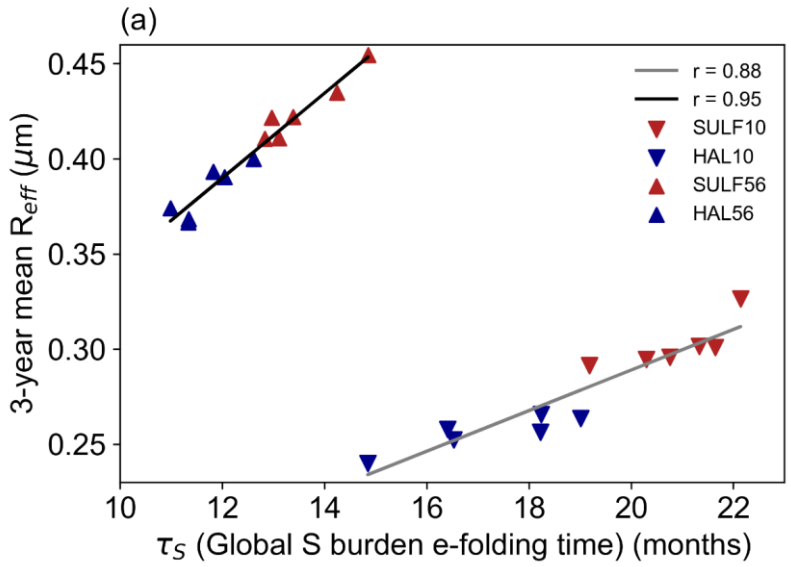

Figure 3 Global-mean aerosol effective radius over the first 3 post-eruption years as a function of the global total sulfur e-folding time. **(a)** SULF56 and HAL56, **(b)** SULF56 and HAL56. Both plots have regression lines fitted with correlation coefficient (*r*) showing strong positive correlation.

The radiative impact of sulfate aerosols depends on the particle size (Timmreck *et al.*, 2010). Using Mie scattering theory, Lacis (2015) found that the scattering cross section per unit mass is largest for sulfate aerosol with effective radius of ~0.20 µm. The smaller R_{eff} in HAL10 and HAL56, compared to SULF10 and SULF56, is closer to 0.20 µm and results in more efficient scattering of SW radiation per unit mass (Timmreck *et al.*, 2010). Therefore, we simulate 11% and 22% higher peak global-mean SAOD anomalies at 550 nm in HAL10 and HAL56 than their equivalent SULF simulations (Figure 4), despite having a 14% and 9% smaller peak aerosol burden. Correspondingly, we simulate an 8% and 6% increase in the peak global-mean ERF_{ari} in HAL10 and HAL56 compared to SULF10 and SULF56 (Figure 4), driven by a 14% and 11% increase in peak global-mean SW forcing (Figure S4). The SAOD and ERF_{ari} anomalies are a balance between the offsetting effects of smaller aerosol and shorter lifetime which result in a net-zero impact on cumulative ERF_{ari} despite a significant increase in the peak global-mean ERF_{ari} (Figure S5).

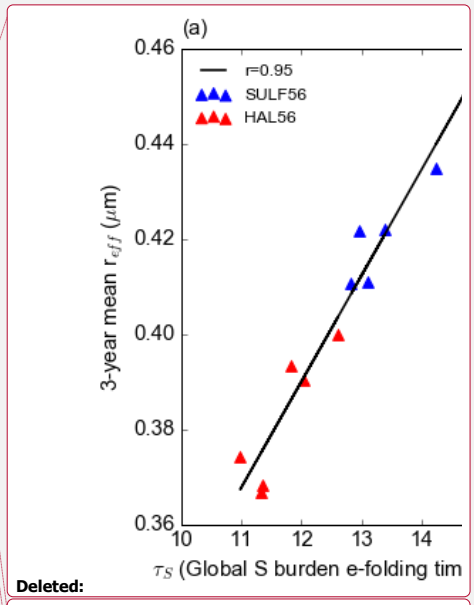

Deleted:
Deleted:
Deleted: r
Deleted: (
Deleted: ,
Deleted: 5
Deleted: 5
Deleted: of
Deleted: stratospheric aerosol optical depth (
Deleted: (Figure 4).
Deleted: d
Deleted: 2a,b

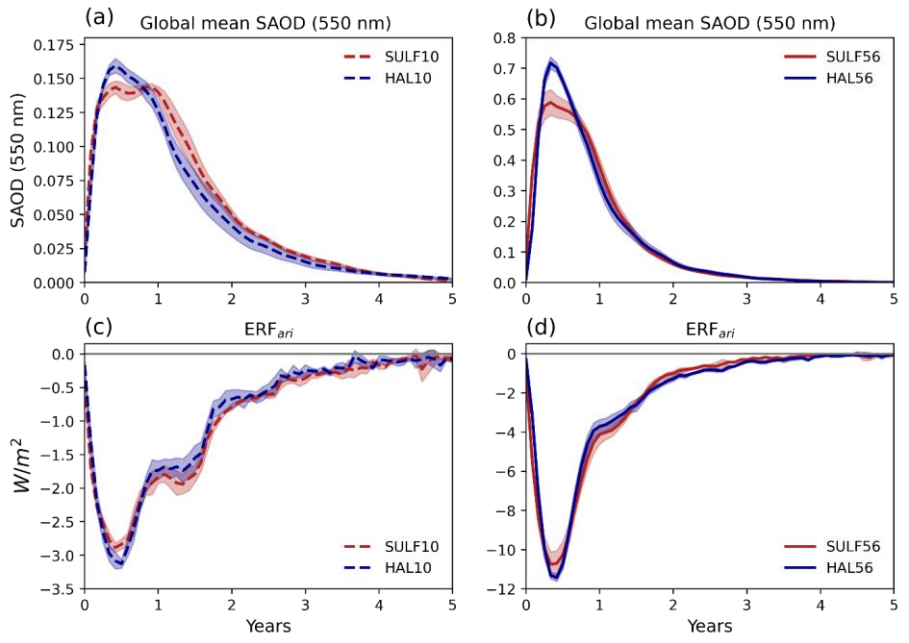

Figure 4 Global-mean evolution of the stratospheric aerosol optical depth anomaly at 550nm, **(a)** SULF56 and HAL56, **(b)** SULF10 and HAL10. Global-mean evolution of top of atmosphere global-mean ERF$_{ari}$ **(c)** SULF56 and HAL56, **(d)** SULF10 and HAL10. Shading represents the ensemble range.

3.2 Composition Changes and Resulting ERF$_{clear,clean}$

Co-emission of volcanic sulfur and halogens causes significant perturbations to the chemistry of the stratosphere beyond the depletion of OH in HAL10 and HAL56 mentioned in section 3.1. Stratospheric methane, stratospheric water vapour (SVW) and, in particular, stratospheric ozone are all impacted.

In sulfur-only simulations, we simulate a modest reduction in global-mean ozone column, -9 DU (-3.9%) in SULF10 and -15 DU (-6.6%) in SULF56 (Figure 5a,c). This ozone depletion is catalysed by halogen radicals activated from background halogens on the surface of volcanic aerosol. We also simulated a redistribution of tropical ozone, with decreases of <0.5 and <2 ppmv between 23 to 28 km and a symmetrical increase in zonal-mean tropical ozone above in SULF10 and SULF56 respectively (Figure 6a,c). This tropical ozone dipole pattern is mostly attributed to volcanic heating. Volcanic heating by the aerosol increases the vertical ascent, and brings ozone up from below enhancing the local mixing ratio. In simulations with co-emitted halogens we simulate more dramatic ozone depletions; HAL10 resulted in a peak global-mean ozone reduction of 65 DU (-22%) 1-2 years after the eruption followed by a gradual recovery over the next 3-4 years (Figure 5d). HAL56 resulted in a peak global-mean ozone reduction of 175 DU (-57%) 1-2 years after the eruption followed by a gradual recovery the

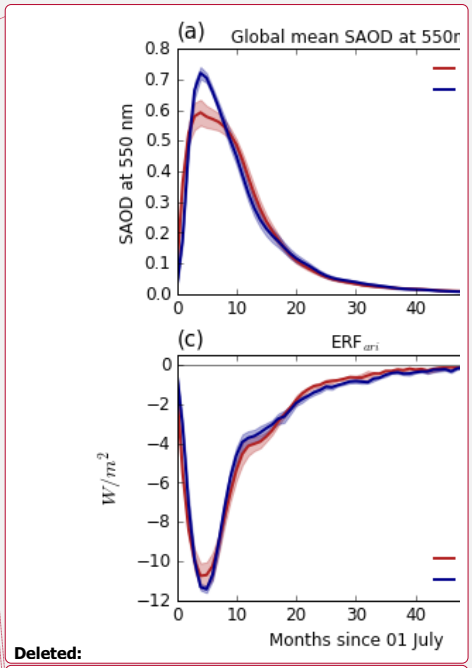

Deleted:

Deleted: SAOD

Deleted: .

remainder of the 10-year simulation, with an average reduction of 82 DU (-27%) over the 10-year simulation (Figure 5b).

Volcanic halogen catalysed ozone depletion was simulated across all latitudes, but the largest magnitude changes in HAL10 (-40%) and HAL56 (-80%) were within the aerosol cloud and the polar regions, where the co-emitted halogens were activated on aerosol surfaces and PSCs respectively (Figure 5). Ozone depletion predominantly occurs in the tropics between 25 and 30 km in the first post-eruption year, with depletion maxima of -3.5 ppmv and -6 ppmv in HAL10 and HAL56 respectively (Figure 6). By year three, the ozone depletion shows a similar bimodal altitude distribution in the stratosphere similar to that found in Brenna *et al*. (2020), with depletion maxima both in the lower (20 km) and upper (40km) stratosphere. As the volcanic SO_2 and halogens were introduced into the stratosphere just south of the equator, they were predominantly dispersed into the southern hemisphere (Figure S6), leading to larger ozone depletions compared with the northern hemisphere. In both HAL10 and HAL56 tropical ozone was found to recover first with significant depletions recurring during the winter in the polar regions for the remainder of the simulation.

The simulated changes in stratospheric heating following sulfur-only and co-emission eruption scenarios affect the dynamical response of the upper atmosphere, for example, the strength of the Arctic and Antarctic polar vortices (see Figure S7) (Robock, 2000; Toohey *et al.*, 2014). In SULF10 and SULF56, the positive stratospheric temperature anomalies in the tropics lead to an increased meridional temperature gradient. As a result, we simulated a strengthening of the polar vortex (defined as mean zonal wind speed at the vortex edge, between 55° - 65° latitude and 1 to 30 hPa) in both the Arctic and Antarctic in the first post-eruption winter. In contrast, the negative stratospheric temperature anomalies in HAL10 and HAL56, lead to a decreased meridional temperature gradient and a weakening of the polar vortices. In HAL10 we simulated significant weakening of the polar vortex in the first two post-eruption winters in the Arctic, and the first and third post-eruption winter at the Antarctic. In HAL56, we simulated significant weakening of the polar vortex for 3-4 years at both poles. Polar vortex strength is an important driver of ozone depletion, with stronger polar vortexes leading to enhanced ozone depletion (Solomon, 1999; Zuev and Savelieva, 2019). Lawrence *et al.* (2020) linked an unusually strong Arctic polar vortex with the record-breaking ozone loss observed in the 2019/2020 Arctic winter. As such, the strengthening of the polar vortices simulated in sulfur-only simulations may intensify ozone depletion in the first post-eruption winters in both the Arctic and Antarctic. Furthermore, the weakening of the polar vortices simulated in co-emission scenarios may dampen the ozone response in both the Arctic and Antarctic. In addition, the simulated changes in polar vortex strength may have important consequences for the North Atlantic Oscillation and Southern Annular Mode (Driscoll *et al*., 2012; Jones *et al*, 2020; Kwon *et al*,. 2020).

Deleted:

Deleted:

Deleted: Ozone depletion shows a similar bimodal altitude distribution in the stratosphere similar to that found in Brenna *et al*., (2020), with 3 year mean depletion maxima (-1 ppmv and -3.5 ppmv in HAL10 and HAL 56) in the lower (20 km) and upper (40km) stratosphere (Figure 6).

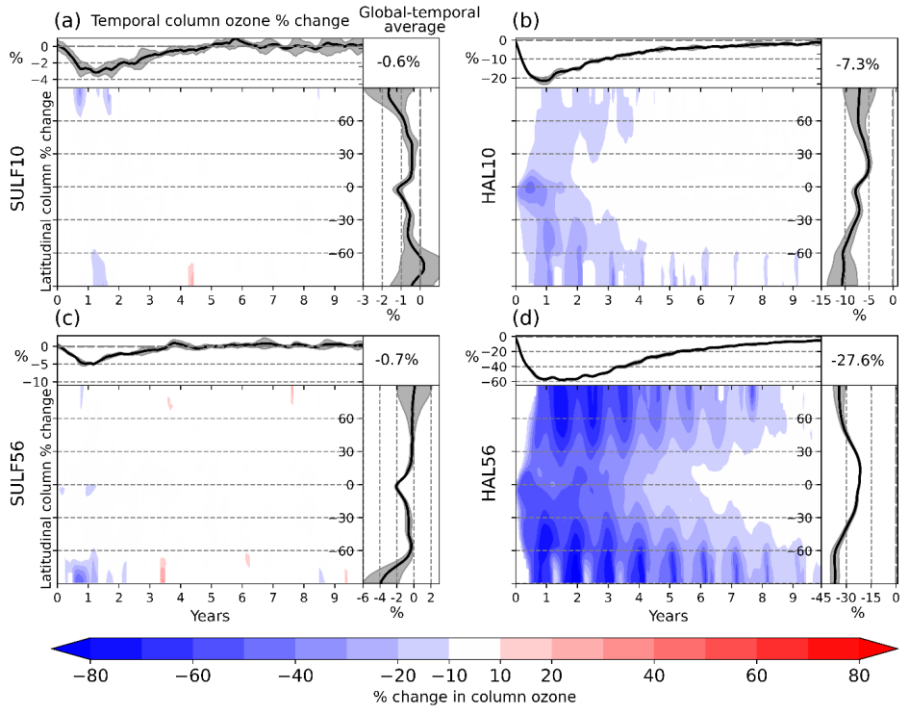

Figure 5 Ozone percentage difference in response to the simulated volcanic eruptions **(a)** SULF56, **(b)** HAL56, **(c)** SULF10, **(d)** HAL10. Global averages of total column ozone perturbation are traced atop each panel as a function of time. Temporal average ozone anomalies are traced right, note different scales. Global-temporal averages are enumerated in the top right. Red colours indicate column ozone enhancement, and blue colours indicate column ozone depletion. Grey shaded areas represent the ensemble range.

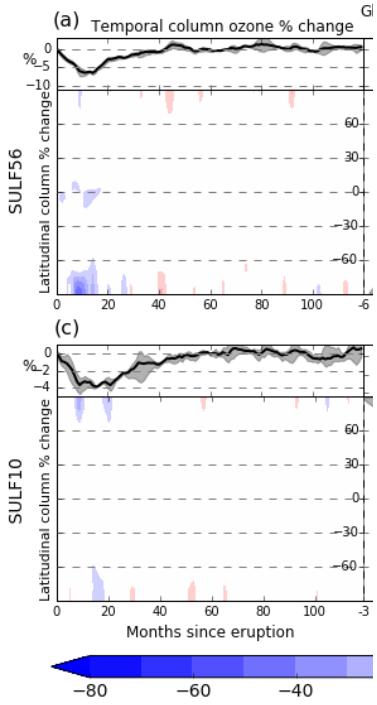

Deleted:

Deleted: ¶

Deleted: %

Deleted: colors

Deleted: colors

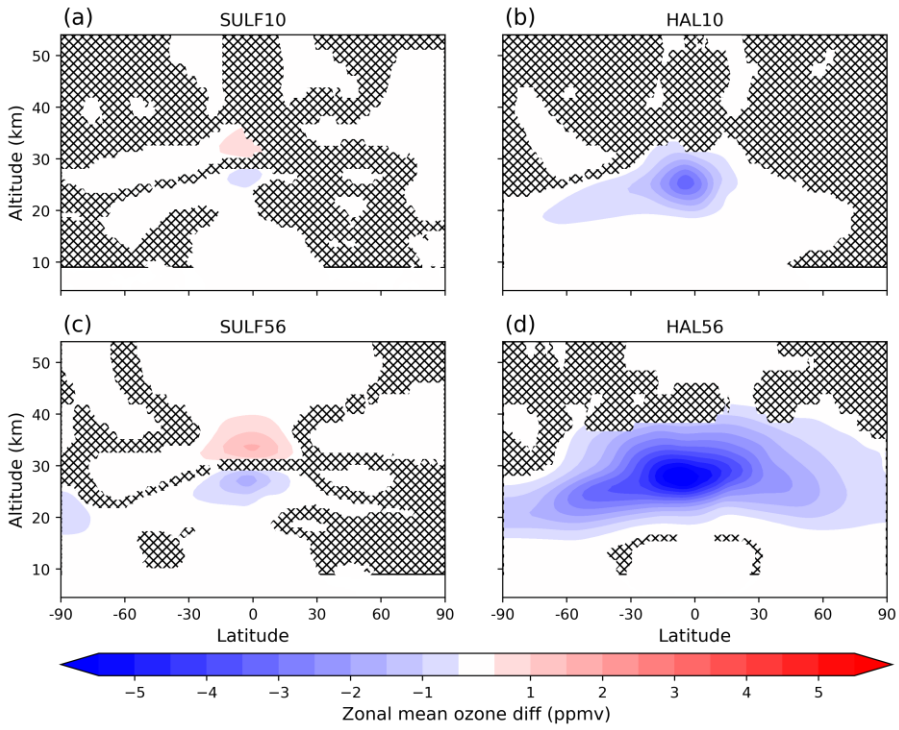

Figure 6 Zonal-mean difference in ozone (ppmv) averaged over the first post-eruption year relative to the control climatology. **(a)** SULF56, **(b)** HAL56, **(c)** SULF10, **(d)** HAL10. Red colours indicate ozone enhancement, and blue colours indicate ozone depletion. Differences that are not significant at the 95% confidence interval according to a Mann–Whitney U test are indicated with stipples.

Stratospheric water vapour (SWV) and stratospheric methane are linked. SWV has two main sources: transport from the troposphere and chemical production from methane (Löffler *et al.*, 2016). By contrast, stratospheric methane's only source is transport from the tropics and it is destroyed by OH (forming SWV) and reaction with halogens via equation 5.

$$Cl + CH_4 \rightarrow HCl + CH_3 \qquad \text{Eq. 5}$$

Following sulfur-only eruptions we simulate small enhancements in SWV and stratospheric methane (Figure 8). SULF10 and SULF56 result in a peak global stratospheric mean increase in SWV of 0.4 ppmv (+7%) and 1.1 ppmv (+17%) and a 10 ppbv (0.6%) and 30 ppbv (1.8%) increase in stratospheric methane respectively. Perturbations to SWV and stratospheric methane peak 2-3 years after the eruption and recover within 7 years. The increase in stratospheric methane following sulfur-only eruptions is in broad agreement with both Loffler (2015),

Deleted: Following sulfur-only eruptions we simulate small enhancements in stratospheric water vapour (SWV) and methane (Figure 8). SULF10 results in a peak increase in SWV of 0.4 ppmv (+7%) and a 10 ppbv (0.8%) increase in stratospheric methane 3- ...

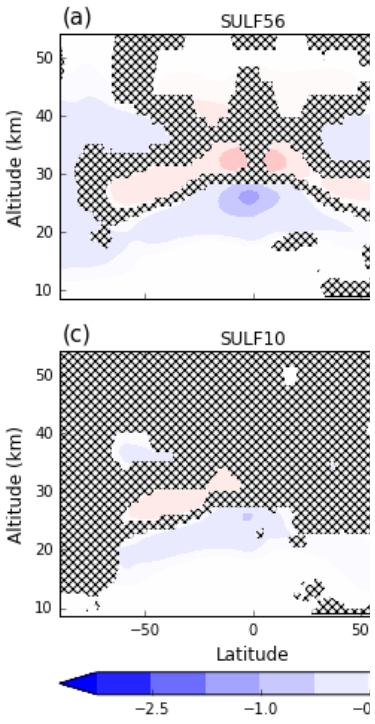

Deleted: ...

Deleted:

Deleted: 3 years

Deleted:

Deleted:

Deleted: colors

Deleted: colors

Deleted: Stratospheric water vapour (

Deleted:)

Field Code Changed

Deleted: ;

Deleted: S

Deleted: sourced from

Deleted: oxidation via

Deleted: to

Deleted: .

Deleted: 2

Deleted: ¶
Sulfur-only eruptions cause an increase in the levels of stratospheric methane, in agreement with Loffler et al. (2015), who showed ...

who showed stratospheric methane mixing ratios increased by ~5% following simulations of El Chichón and 15-20% following the larger Mt Pinatubo and (Kilian *et al.*, 2020), who reported a 10% increase in CH_4 between 40 and 10 hPa, also following simulations of Pinatubo. Killian *et al.* (2020) suggested that this was due to enhanced vertical ascent as a result of aerosol heating, lifting relatively methane-rich air from the lower stratosphere into the upper levels. As Kilian *et al.* (2020) simulated an increase in stratospheric CH_4 burden, they suggested that the lofting of methane must also coincide with an increase in the stratospheric methane lifetime but did not calculate this. In SULF10 and SULF56 of this work, we simulate an increase in tropical vertical ascent (shown at 50 hPa in Figure S2), however, we simulate a coinciding reduction in the stratospheric methane lifetime, driven by an increase in methane oxidation by OH and Cl. (Figure S8). This suggests that the increased stratospheric methane burden following sulfur-only eruptions SULF10 and SULF56 is not due to a lengthening of the stratospheric methane lifetime and, instead, is likely due to increased transport of methane across the tropopause from the methane rich troposphere as a result of increased vertical ascent in the stratosphere (Figure S2). Due to the model set up employed in this study we were unable to diagnose this any further.

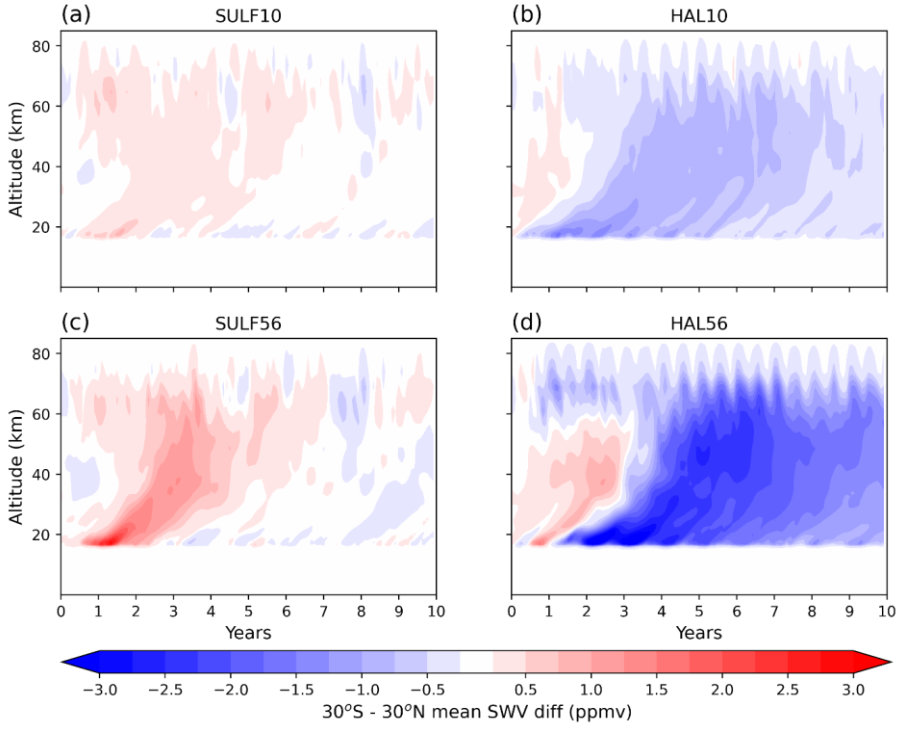

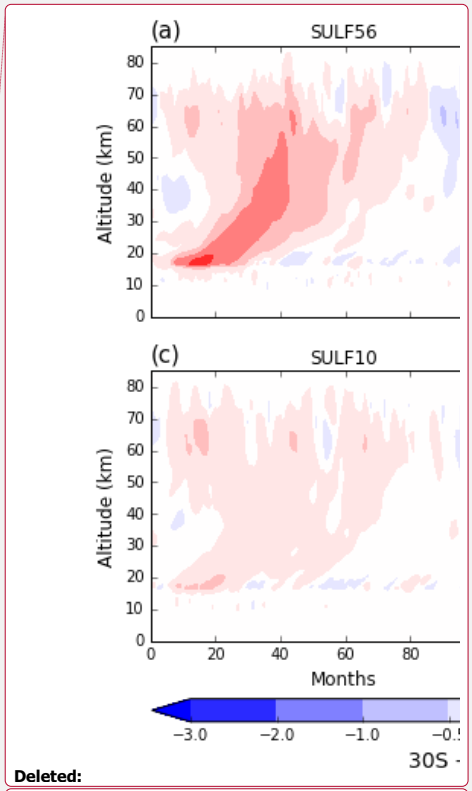

Figure 7 30°S - 30°N mean difference in stratospheric water vapour (ppmv) relative to the control climatology as a function of altitude and time, **(a)** SULF56, **(b)** HAL56, **(c)** SULF10, **(d)** HAL10. Red colours indicate SWV enhancement, and blue colours indicate column SWV depletion.

Deleted:
Deleted: M
Deleted: SWV
Deleted: colors
Deleted: colors
Deleted: ozone

The simulated changes in methane are small in comparison to the SWV changes across all simulations and can only account for a fraction of the SWV change. The dominant driver of SWV change is the amount of water vapour entering the stratosphere through the tropical tropopause cold point ((Löffler *et al.*, 2016). Following both SULF10 and SULF56 volcanic aerosol resulted in warming of the tropical tropopause cold point leading to an increase in vertical ascent (Figure S2) and a weakening of the tropical tropopause cold trap dehydration effect, increasing the transport of water vapour into the stratosphere (Figure 8) (Loffler *et al.*, 2016). Elevated SWV is seen to initiate at the tropical troposphere before propagating higher into the stratosphere (Figure 7a,c).

Unlike in sulfur-only eruptions, following eruptions with co-emitted halogens we simulate a reduction in SWV and stratospheric methane (Figure 8). HAL10 and HAL56 result in a peak global stratospheric mean stratospheric methane reduction of 37 ppbv (-3%) and 214 ppbv (-18%) respectively 2 years after the eruption. In HAL10 the stratospheric methane perturbation returns to the background levels over 3-4 years whereas in HAL56 the perturbation remains below zero for between 7-8 years. Co-emission of halogens results in enhanced destruction of methane by chlorine via Eq. 5 resulting in the significant decrease in the HAL10 and HAL56 stratospheric methane levels.

HAL10 and HAL56 result in a peak SWV reduction of 1.0 ppmv (-16%) and 2.3 ppmv (-36%) respectively 3-4 years after the eruption followed by a gradual recovery. In HAL10 SWV perturbation levels return to the background levels over 6-7 years whereas in HAL56 the perturbation does not fully recover within the 10-year duration of the simulation. Just as was the case following sulfur-only eruptions, the dominant driver of SWV changes is the amount of water vapour entering the stratosphere via the tropical tropopause cold point. In HAL10 and HAL56, the process is the same but in the opposite sense. Cooling in the tropical tropopause vicinity increases the efficiency of the tropical cold trap dehydration effect and reduces the amount of water vapour being brought up from the troposphere (Figure 8) (Loffler *et al.*, 2016). The negative SWV anomalies can be seen to initiate at the troposphere before propagating higher into the stratosphere (Figure 7b,d)

Deleted: The simulated changes in methane are small in comparison to the SWV changes across all simulations and thus can only account for a fraction of the SWV change. Both with and without halogens, the dominant driver of SWV change is the amount of water vapour entering the stratosphere through the tropical tropopause (Loffler et al., 2016). SULF10 and SULF56 resulted in elevated SWV as volcanic aerosol heating lead to more air being brought from the troposphere and a weakening of the tropical tropopause cold trap dehydration effect (Figure 8) (Loffler et al., 2016). Elevated SWV is seen to initiate at the tropical troposphere before spreading higher into the stratosphere (Figure 7a,c). In the case of co-emitted halogens, the process is the same but in the opposite sense. Cooling in the tropical tropopause vicinity reduces the amount of water vapour being brought up from the troposphere and increases the efficiency of the tropical cold trap dehydration effect (Figure 8) (Loffler et al., 2016). The negative SWV anomalies can be seen to initiate at the troposphere before spreading higher into the stratosphere (Figure 7b,d).¶

Field Code Changed

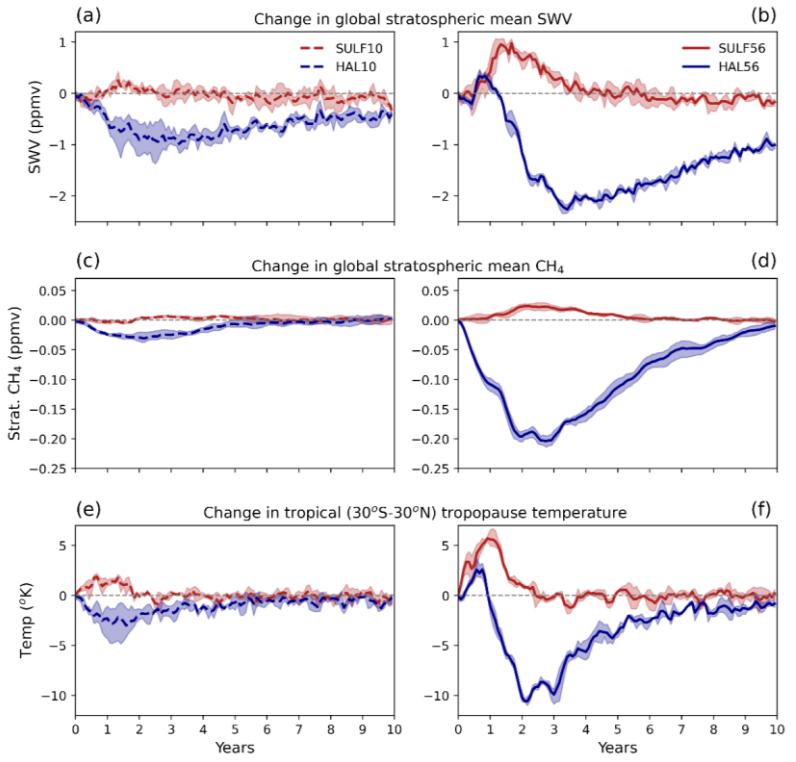

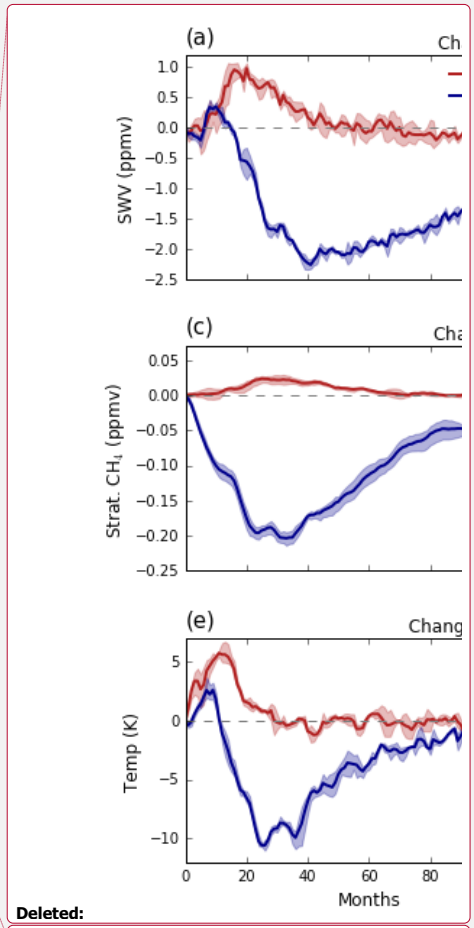

Figure 8 Evolution of global stratospheric mean water vapour (ppmv) in SULF56 and HAL56 **(a)**, and SULF10 and HAL10 **(b)**. Evolution of global stratospheric methane (ppmv) in SULF56 and HAL56 **(c)**, and SULF10 and HAL10 **(d)**. Evolution of tropical tropopause cold trap temperature difference averaged over 30°S–30°N and 15-20 km in SULF56 and HAL56 **(e)**, and SULF10 and HAL10 **(f)**. Shading represents the ensemble range.

Using the forcing diagnosis outlined in Schmidt *et al.* (2018) and Ghan (2013), we can isolate the radiative forcing due to atmospheric composition and surface albedo changes, $ERF_{clear,clean}$. As surface temperature and sea ice were prescribed, surface albedo changes were small, meaning that $ERF_{clear,clean}$ predominantly represents the forcing from atmospheric composition changes (Figure 9 c, d). HAL10 results in a peak global-mean $ERF_{clear,clean}$ of -1.3 Wm^{-2} one year after the eruption, more than double the $ERF_{clear,clean}$ of SULF10. The forcing recovers gradually over the next 6-7 years and results in a cumulative $ERF_{clear,clean}$ that is 5 times greater than SULF10 (Figure S2d). Similarly, HAL56 results in a peak global-mean $ERF_{clear,clean}$ of -2.1 Wm^{-2} 1-2 years after the eruption, double the peak global-mean forcing of SULF56. The $ERF_{clear,clean}$ anomaly in HAL56 is more persistent and remains -0.5 Wm^{-2} below zero at the end of the simulation, resulting in a cumulative $ERF_{clear,clean}$ that is 10 times greater than SULF56 (Figure S2c).

Deleted:
Deleted:
Formatted: Superscript
Deleted: -
Deleted: (
Deleted: ,
Deleted: (
Deleted: ,
Deleted: Ghan (2013)
Deleted: we prescribe
Deleted: are assumed to be unchanged
Deleted: r
Deleted: 10

To calculate the resulting radiative forcing of the simulated ozone changes we use the ozone radiative kernel (O_3 RK) technique based on Rap *et al.* (2015) and updated for the whole atmosphere as outlined in Iglesias-Suarez *et al.* (2018 (Figure S9). The O_3 RK is constructed by calculating the change in LW and SW flux caused by a 1 ppb perturbation in ozone added to each atmospheric layer in turn. The change in SW and LW flux is diagnosed using the offline version of the Suite Of Community RAdiative Transfer (SOCRATES) model, based on Edwards and Slingo (1996). The LW component of the O_3 RK (Fig. S9c) is positive throughout the atmosphere, with a maximum in the tropical upper troposphere lower stratosphere. The SW component (Fig. S9c) is negative above ~12km altitude and positive below ~12km altitude. This results in a net O_3 RK (Fig. S9a) which is positive everywhere except above ~25km between 60°S and 60°N. Using the O_3 RK, we are able to show that the stratospheric ozone change is the dominant driver of the $ERF_{clear,clean}$ accounting for ~75% of the $ERF_{clear,clean}$ (Figure 9a,b). The remainder is likely predominantly due to SWV changes with a small contribution from stratospheric methane changes. The latitudinal pattern of ozone radiative forcing reflects the locations of the ozone change, with largest forcing at the poles, as shown in Figure S10 and S11.

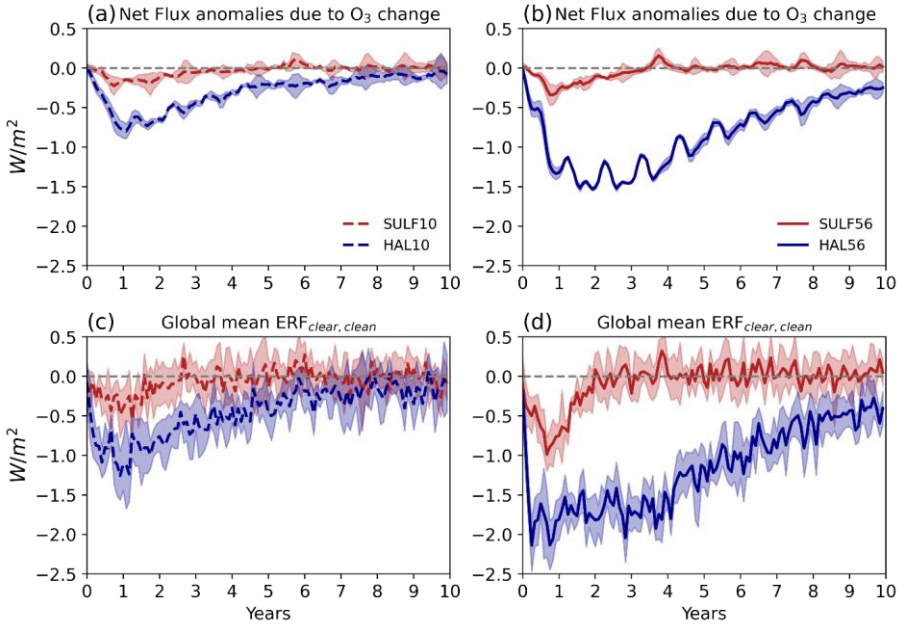

Figure 9 Evolution of global-mean top of atmosphere net flux anomalies due to stratospheric O_3 change, in SULF56 and HAL56 estimated from the ozone radiative kernel from Rap *et al*. (2015) **(a)**, SULF10 and HAL10 **(b).** Evolution of the global-mean top of atmosphere compositional forcing ($ERF_{clear,clean}$) in SULF56 and HAL56 **(c)**, SULF10 and HAL10 **(d)** Ozone changes make up ~75% of the $ERF_{clear,clean}$. Shading represents the ensemble range.

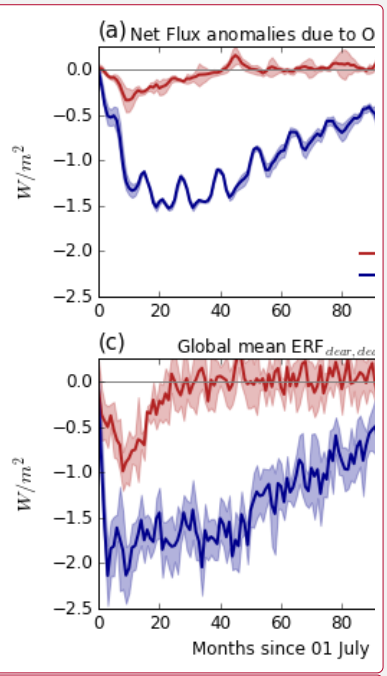

Deleted:

Deleted: whole atmosphere ozone radiative kernel from Rap et al., 2015

Deleted:

Deleted:

Deleted: TOA

4 Discussion

Using the Ghan (2013) method for diagnosing forcing, we have shown that the co-emission of volcanic halogens results in larger peak global-mean ERF_{ari} and $ERF_{clear,clean}$. Taking these in combination, the co-emission of halogens results in substantial increases in the peak global-mean volcanic ERF to -4.1 Wm^{-2} (+30%) in HAL10, and -14.1 Wm^{-2} (+24%) in HAL56 (Figure 10a,b), as well as increases in the total cumulative forcing to -1.37 $x10^{23}$ J (+60%) in HAL10 and -3.86$x10^{23}$ J (+100%) in HAL56 compared to SULF10 and SULF56 (Figure S5e,f). In both HAL10 and HAL56, ~25% of the additional peak global-mean volcanic ERF simulated compared to SULF10 and SULF56 respectively comes from the changes to the ERF_{ari}, with the remainder coming from changes to $ERF_{clear,clean}$.

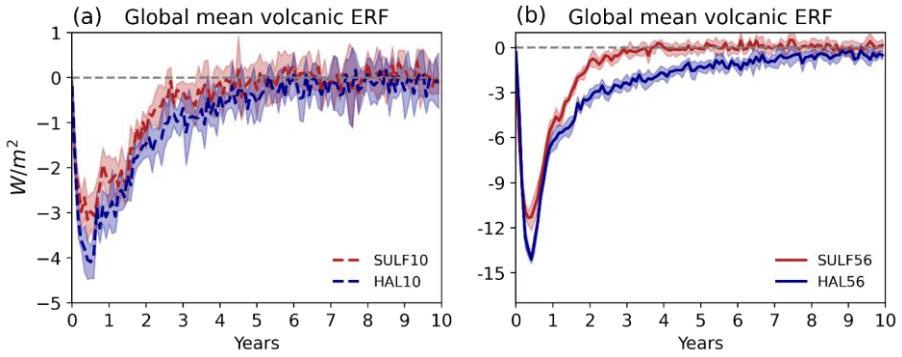

Figure 10 Evolution of the global-mean top of atmosphere total volcanic forcing ERF forcing (volcanic ERF) relative to the control climatology in SULF56 and HAL56 **(a)**, SULF10 and HAL10 **(b).** Volcanic ERF is the sum of ERF_{ari} , ERF_{acii} and $ERF_{clear,clean}$. Shading represents the ensemble range.

Comparing the perturbations in HAL56 to HAL10, we find that increasing the volcanic halogen flux by 10 times only results in a ~2.5 times larger global ozone response and, as $ERF_{clear,clean}$ is dominated by changes in stratospheric ozone, only a ~2 times larger $ERF_{clear,clean}$. This suggests that there is a saturation in the ozone depleting potential of co-emitted volcanic halogens. Plotting the column ozone percentage change against the magnitude of injected halogens expressed as Equivalent Effective Stratospheric Chlorine (EESC is a measure of the ozone destruction potential; $EESC=[Cl]_{added\ to\ stratosphere} + 60 \times [Br]_{added\ to\ stratosphere}$; Cadoux *et al.*, 2015) from this study and a number of previous studies, we find an exponential decay curve describes this relationship: as the EESC increases the efficiency of volcanic halogen ozone depletion decreases (Figure 11). This relationship suggests that column ozone is most sensitive to volcanic halogens when the additional EESC is < 20 Tg, and that increasing the volcanic EESC flux beyond 60 Tg has little impact on column ozone change. This analysis spans simulations with very different background EESC and column ozone values. Wade *et al*. (2020), Brenna *et al*. (2019), and Brenna *et al*. (2020) simulations are all in a pre-industrial atmosphere background states with low background chlorine levels, whereas, the background chlorine levels in HAL10 and HAL56 are significantly higher and with lower initial ozone columns. This relationship suggests that the peak global-mean ozone loss (%) is dependent more on the volcanically injected EESC than the background chlorine and initial ozone columns. In other words, this relationship is time-independent and this exponential decay curve can be used to estimate the

Deleted: 2

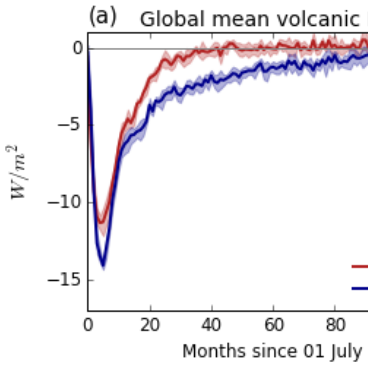

Deleted: ¶

Deleted:

Deleted: the

peak global-mean ozone loss for an eruption in any climate state, including future eruptions where the background EESC will have decayed back to pre-1980s levels. This will be especially useful for rapid estimates of ozone change as new or better constrained volcanic halogen data becomes available.

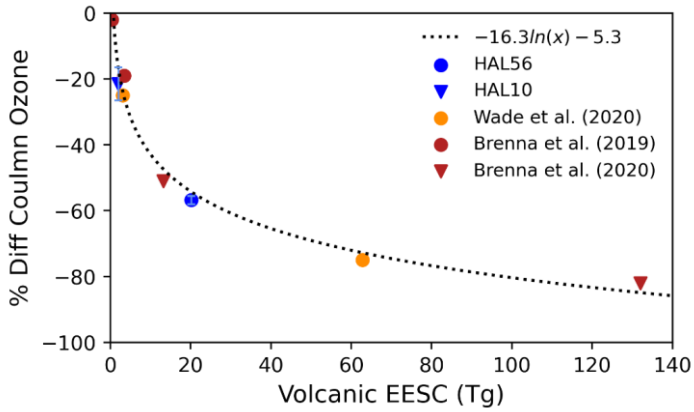

Figure 11 Relationship between volcanically emitted Equivalent Effective Stratospheric Chlorine and peak global-mean % difference in column ozone. Blue : HAL10 and HAL56 ensemble mean and range. Orange : Wade *et al.* (2020) ensemble mean. Red : Brenna *et al.* (2019) and Brenna *et al.* (2020) ensemble mean.

The implications of ozone depletion in HAL10 and HAL56 go further than enhancing the $ERF_{clear,clean}$. High anthropogenic fluxes of halocarbons into the atmosphere during the 1980s caused background chlorine levels to be elevated during the 1990s and an ozone hole is simulated to develop in the polar region every SH winter (Figure S12) of our control simulation. Using the definition for ozone hole conditions as <220 DU, we simulate enhanced ozone hole conditions following both HAL10 and HAL56 eruptions (Figure 12). In HAL10, ozone hole conditions are simulated in the tropics for one year after the eruption, and a deepening of ozone hole conditions is seen in northern hemisphere polar regions for two winters and in the southern hemisphere polar regions for four winters. In HAL56, we simulate ozone hole conditions globally for 5 years, continuing for a further three winters in the NH polar regions and six winters in the SH polar regions.

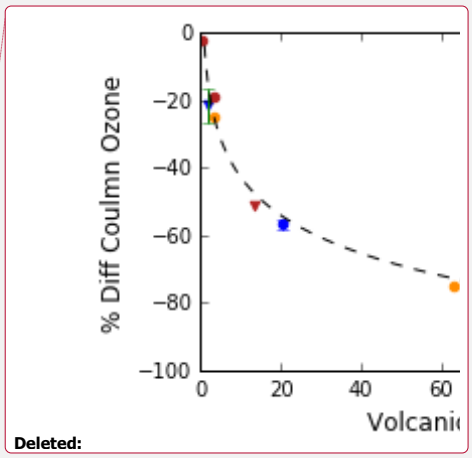

Deleted:

Deleted: EESC

Deleted: (Cl + 60*Br (Tg))

Deleted: Green

Deleted: ,

Formatted: Font: Italic

Deleted: ,

Deleted:

Deleted: 4

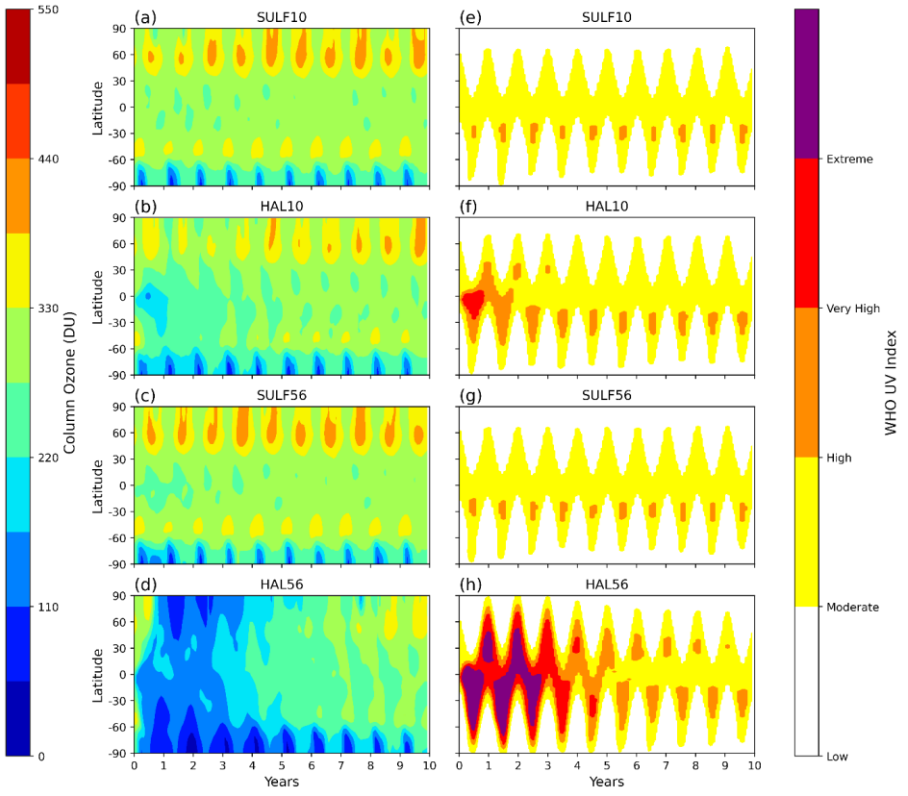

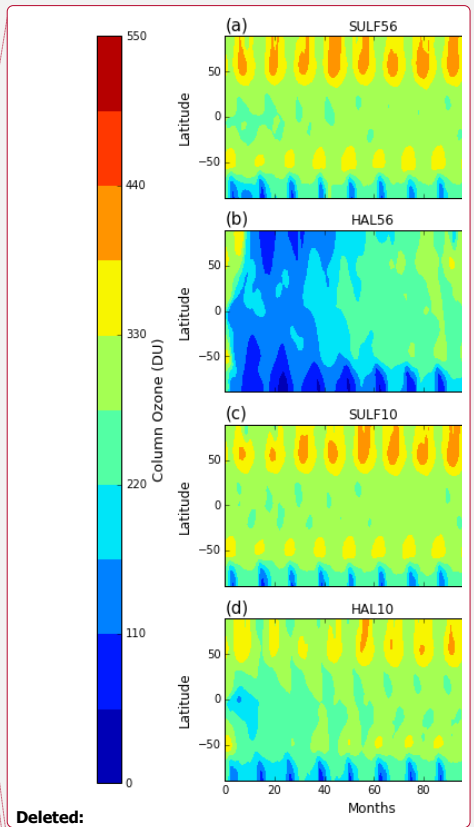

Figure 12 Zonal-mean column ozone **(a)** SULF56, **(b)** HAL56, **(c)** SULF10, **(d)** HAL10. Ozone hole conditions are simulated when the column ozone < 220 DU. Zonal-mean surface UV exposure due to column ozone change (WHO UV Index) **(e)** SULF56, **(f)** HAL56, **(g)** SULF10, **(h)** HAL10.

Column ozone depletion on this scale would dramatically increase the flux of harmful UV to the surface, which could cause DNA damage to animals and plants, and increase the occurrences of skin cancers, eye damage and immune system deficiencies among the population (World Health Organisation (WHO), 1994). Climate modelling and environmental proxies showed that ozone depletion as a result of halogen degassing during the emplacement of Siberian Traps flood basalts lead to ozone depletion that stressed ecosystems and caused DNA mutations which may have contributed to the end-Permian mass extinction (Black *et al.*, 2014). A simple heuristic relating column ozone to clear-sky surface UV index is given by:

$$UV\ Index\ =\ 12.5\mu_o^{2.42}(\Omega/300)^{-1.23}$$

Deleted:

Deleted:

Deleted:

Deleted: modeling

as defined in (Madronich, 2007), where μ_o is the cosine of the solar zenith angle and Ω is the total vertical ozone column in Dobson units. The monthly mean average UV index coloured by World Health Organization categories (Low [0 to 2], Medium [3 to 5], High [6 to 7], Very High [8 to 10], and Extreme [11+]) is shown in Figure 12. This shows that in the HAL56 scenario, on average 'Very High' or 'Extreme' UV levels would be expected all day for much of the globe in the three to four summers after the eruption, with noon values being even higher. The change in surface UV levels are shown in Figure S13. Living under such a high UV exposure would cause immediate immunosuppression, epidemic outbreaks, increases in the occurrences of eye damage and, in the longer term, skin cancers among the population living between the equator and the mid-latitudes, which equates to >95% of the global population. The assessment of surface UV changes is made more challenging by the presence of volcanic aerosols, which also scatter UV radiation. However, damaging UVB and UVC radiation will not be scattered effectively by larger aerosol size distributions and volcanic aerosol levels reduce rapidly after peaking in the first post-eruption year.

Whilst we have been able to calculate the composition and climate impacts of the co-emission of halogens and SO_2 from volcanic eruptions, these calculations are not without some uncertainty. Recent studies carried out as part of the Volcanic Forcings Model Intercomparison Project (VolMIP) showed large model response disparities in simulations of SO_2-only volcanic eruptions (Clyne *et al.*, 2021), but models have been shown to capture the effects of ozone depleting substances on stratospheric ozone well (World Meteorological Organization (WMO), 2014). As outlined in the introduction, the major uncertainty in this work is the stratospheric injection of HCl and HBr from explosive volcanic eruptions, which is highly variable and depends on both the geochemistry of the volcano and the degree of scavenging determined by the prevailing atmospheric conditions during the eruption. It is clear, however, that significant stratospheric halogen fluxes occur after some explosive volcanic eruptions.

Although this work has focused on simulations of explosive volcanic eruptions in a background climate representative of the 1990s, Figure 11 demonstrates the simulated ozone depletion predominantly depends on the volcanic halogen injection size and not the background atmospheric state. Using the relationship outlined in Figure 11, we can estimate the peak global-mean ozone percentage loss for any size of volcanic halogen injection, past or present. We are currently investigating the impacts that plausible future background atmospheric states (such as different greenhouse gas concentrations, background halogen levels and stratospheric temperatures) may have on the simulated ozone response and volcanic ERF due to co-emitted sulfur and halogen volcanic emissions.

In addition to the co-emission of volcanic halogens, there is also scope to model the co-emission of volcanic water vapour and ash directly into the stratosphere. Legrande *et al.* (2016) provided a mechanism explaining how SWV originating from volcanic eruptions may alter the chemistry of the stratosphere and the nucleation rate of sulfate aerosol, and suggested that this may severely alter the climate impacts. In addition, SVW proved to be an amplifying feedback in simulations in this work and it would be interesting to see how co-emission of water vapour, halogens and sulfur would further alter the volcanic forcing in simulations of explosive volcanic eruptions. Zhu *et al.* (2020) showed the importance of including volcanic ash injections in climate simulations. When heterogeneous chemistry on ash particles was included they found that 43% more volcanic sulfur was removed

Deleted: It is worth noting, that t

Deleted: plan to

Deleted: explore this more and understand

from the stratosphere in the first 2 months. Volcanic ash is also likely to alter the lifetime, activation and impact of co-emitted volcanic halogens in climate simulations.

5 Conclusions

In this study we utilised UKESM-AMIP simulations of volcanic eruptions to investigate how the co-emission of volcanic halogens and sulfur alters the effective radiative forcing (ERF) of explosive volcanic eruptions under atmospheric conditions representative of the mid-1990s. As the volcanic flux of HCl and HBr into the stratosphere remains uncertain, a range of plausible explosive volcanic emissions scenarios based on petrological degassing estimates, satellite observations and volcanic plume modelling were simulated. The four sets of experiments included one large SO_2 (10 Tg), and one very-large SO_2 (56 Tg) emission scenario, both with (HAL10 and HAL56) and without halogens (SULF10 and SULF56), each with an ensemble size of 6 sampling different QBO states. These eruption sizes (10 and 56 Tg SO_2) are hypothetical, but they are comparable to a VEI 6 (e.g. 1991 Mt. Pinatubo) and a VEI 7 (e.g. 1257 Mt. Samalas) eruption, representing 1 in 50-100 year and 1 in 500-1000 year events respectively. HAL56 utilises the 1257 Mt. Samalas HCl and HBr emission estimates from Vidal *et al.* (2016) and assumes a conservative ~5% stratospheric halogen injection efficiency. HAL10 has a SO2 injection similar to that found to reproduce the spatial and temporal evolution of SAOD following 1991 Pinatubo (Mills *et al.*, 2016) and a 10 times smaller HCl and HBr flux than HAL56.

We have shown that the co-emission of halogens and sulfur in simulations of explosive volcanic eruptions increases the peak and cumulative volcanic ERF significantly. This is due to a combination of increased forcing from i) volcanic aerosol-radiation interactions (ERF_{ari}) and ii) composition of the stratosphere ($ERF_{clear,clean}$).

Co-emitting halogens results in a larger global-mean ERF_{ari} in both HAL10 (+8%) and HAL56 (+6%). Ozone depletion catalysed by volcanic halogens leads to stratospheric cooling which offsets the volcanic aerosol heating (SULF10 ≃ 1.5 K, SULF56 ≃ 3.5 K) and results in a net stratospheric cooling (HAL10 ≃ -2 K, HAL56 ≃ -3.5 K). The ozone-induced stratospheric cooling prevents aerosol self-lofting and keeps the volcanic aerosol lower in the stratosphere with a shorter lifetime, resulting in reduced growth via condensation and coagulation and smaller peak global-mean effective radius compared to sulfur-only simulations. The peak global-mean effective radii of the HAL10 and HAL56 sulfate aerosols are found to be 15% and 10% smaller than SULF10 and SULF56 sulfate aerosol, closer to the most efficient radii for radiation scattering per unit mass, ~0.25 μm. Subsequently, we find HAL10 and HAL56 have higher peak global-mean SAOD anomalies (+11%, +22%) and ERF_{ari} (+8% + 6%).

Co-emission of halogens also results in significant perturbations to the stratospheric chemistry and compositional-driven forcing. Stratospheric methane was found to decrease by 3% and 18% and stratospheric water vapour (SWV) was found to reduce by 16% and 36% in HAL10 and HAL56 respectively. The methane reductions were driven by the enhanced destruction flux by volcanic Cl radicals and the SWV changes were attributed to the same stratospheric temperature reductions mentioned previously. Cooling in the tropical tropopause vicinity increased the efficiency of the tropical cold trap dehydration effect, reducing the flux of water vapour from the troposphere to the stratosphere. The most dramatic change in chemistry was found to be in stratospheric ozone. Significant ozone depletions were simulated globally in both HAL10 (22%) and HAL56 (57%) with prolonged depletion in

Deleted: for

Deleted: high

Deleted: 56

Deleted: l

Deleted: ow

Deleted: 1

Deleted: 0

Deleted: 56

Deleted: 10

Deleted: 56

Deleted: 10

Deleted: 56

Deleted: 10

Deleted: similar in size to

Moved (insertion) [4]

Moved down [3]: VEI 7 (e.g. 1257 Mt. Samalas)

Moved up [4]: VEI 6 (e.g. 1991 Mt. Pinatubo)

Moved (insertion) [3]

Deleted: 0

Deleted: 0

Deleted: HAL10 has a SO_2 injection similar to 1991 Pinatubo and a 10 times smaller injection of HCl and HBr than HAL56. ¶

Deleted: (HAL10 ≃ -2 K, HAL56 ≃ -3.5 K) which more than offsets

Deleted:

Deleted: being transported

both NH and SH winter polar regions. In HAL10, ozone hole conditions (<220 DU) were simulated globally for the first post-eruption year and then for 3-5 years at the poles during the winter. In HAL56, we simulate an ozone hole globally for 5 years followed by a gradual recovery over the following five years until only the polar winters exhibit ozone hole conditions. Stratospheric chemistry changes resulting from the co-emission of halogens increase the peak global-mean $ERF_{clear,clean}$ by ~100% to -2.1 Wm^{-2} in HAL56 and -1.3 Wm^{-2} in HAL10. Stratospheric ozone depletion is the dominant driver of $ERF_{clear,clean}$ accounting for ~75% of the total $ERF_{clear,clean}$.

The total effect of the increased ERF_{ari} and $ERF_{clear,clean}$ is that co-emitting halogens increases the peak global-mean volcanic ERF by 30% and 24% and cumulative ERF by 60% and 100% in HAL10 and HAL56 respectively. Ozone hole conditions exhibited by both HAL10 and HAL56 would result in dramatic increases in the surface UV flux with 'Extreme' UV levels being experienced over most of the globe for 4 years following HAL56 eruptions. UV exposure on this scale would lead to devastating negative consequences for society and the biosphere, including increases in the occurrences of skin cancer, eye damage and immune system deficiencies (WHO, 2002). This work shows for the first time that co-emission of plausible amounts of halogens can amplify the effective radiative forcing in simulations of explosive volcanic eruptions; highlighting the necessity to include volcanic halogens emissions when simulating the climate impacts of past or future eruptions, and the critical need to maintain space-borne observations of stratospheric compounds to better constrain the stratospheric injection estimates of volcanic eruptions.

Deleted: . This h

Deleted: s

Deleted: need

Deleted: fluxes

Deleted: provides motivation to better quantify the degassing budgets and stratospheric injection estimates for volcanic eruptions.

Data Availability

All data required to reproduce our key results are archived in the Centre for Environmental Data Analysis (CEDA) archive, and can be found here: https://catalogue.ceda.ac.uk/uuid/5f4d2f6daebd4195a0368a79405d3686. Post-processing and visualization of data was performed with Python. The scripts and the post-processed data files are available on request from the corresponding author.

Deleted: will be

Author Contributions

J.SS designed the study, ran the UKESM1-AMIP experiments, analyzed the results and wrote the manuscript. A.S. and A.A. provided support for designing the study and analyzing the results. T.A., Y.M.S, J.W., L.R.M., N.L.A. provided support for running the experiments, and T.A., Y.M.S, J.W., provided support for the analysis. All authors contributed to revising the manuscript.

Competing interests.

The authors declare that they have no conflict of interests.

Acknowledgements

JSS and YMS would like to thank NERC through the University of Cambridge ESS-DTP for funding; JW would like to thank the Cambridge Commonwealth, European & International Trust for funding through a Vice

Chancellor's Award. T.J.A. acknowledges support from the Royal Society through a Newton International Fellowship (grant number NIF\R1\180809), from the European Union's Horizon 2020 research and innovation programme under the Marie Skłodowska-Curie grant agreement No 835939, and from the Sidney Sussex college through a Junior Research Fellowship. L.R.M. and A.S. are funded by the U.K. Natural Environment Research Council (NERC) via the "Vol-Clim" grant (NE/S000887/1). In addition, A.S. acknowledges funding via the NERC V-PLUS project (NE/S00436X/1). We would like to thank NERC, through NCAS, and the Met Office for the support of the JWCRP UKCA project. NLA and ATA are supported by NERC and NCAS through the ACSIS project. The team thank NCAS and the Met Office, through the JWCRP, for support of the UKCA model. This work used Monsoon2, a collaborative High Performance Computing facility funded by the Met Office and the Natural Environment Research Council. This work used JASMIN, the UK collaborative data analysis facility. We would like to thank Alex Rap for allowing the use of the ozone radiative kernel and for his help implementing it in this work. Finally, we thank Daniele Visioni, an anonymous reviewer, and Alan Robock whose useful and constructive comments helped to improve and clarify this manuscript.

References

Archibald, A. *et al.* (2020) 'Description and evaluation of the UKCA stratosphere-troposphere chemistry scheme (StratTrop vn 1.0) implemented in UKESM1', *Geoscientific Model Development*. doi: 10.5194/gmd-13-1223-2020.

Bacon, C. R., Newman, S. and Stolper, E. (1992) 'Water, CO2, Cl, and F in melt inclusions in phenocrysts from three Holocene explosive eruptions, Crater Lake, Oregon', *American Mineralogist*.

Black, B. A. *et al.* (2014) 'Acid rain and ozone depletion from pulsed siberian traps magmatism', *Geology*. doi: 10.1130/G34875.1.

Brenna, H. *et al.* (2020) 'The potential impacts of a sulfur- And halogen-rich supereruption such as Los Chocoyos on the atmosphere and climate', *Atmospheric Chemistry and Physics*. doi: 10.5194/acp-20-6521-2020.

Brenna, H., Kutterolf, S. and Krüger, K. (2019) 'Global ozone depletion and increase of UV radiation caused by pre-industrial tropical volcanic eruptions', *Scientific Reports*. doi: 10.1038/s41598-019-45630-0.

Cadoux, A. *et al.* (2015) 'Stratospheric Ozone destruction by the Bronze-Age Minoan eruption (Santorini Volcano, Greece)', *Scientific Reports*. Nature Publishing Group, 5(1), p. 12243. doi: 10.1038/srep12243.

Carn, S. A., Clarisse, L. and Prata, A. J. (2016) 'Multi-decadal satellite measurements of global volcanic degassing', *Journal of Volcanology and Geothermal Research*. doi: 10.1016/j.jvolgeores.2016.01.002.

Clyne, M. *et al.* (2020) 'Model physics and chemistry causing intermodel disagreement within the VolMIP-Tambora Interactive Stratospheric Aerosol ensemble', *Atmospheric Chemistry and Physics*. doi: 10.5194/acp-2020-883.

Deshler, T. *et al.* (1997) 'Stratospheric aerosol following Pinatubo, comparison of the north and south mid

latitudes using in situ measurements', *Advances in Space Research*. doi: 10.1016/S0273-1177(97)00600-5.

Dhomse, S. S. *et al.* (2014) 'Aerosol microphysics simulations of the Mt.∼Pinatubo eruption with the UM-UKCA composition-climate model', *Atmospheric Chemistry and Physics*. doi: 10.5194/acp-14-11221-2014.

Eric Klobas, J. *et al.* (2017) 'Ozone depletion following future volcanic eruptions', *Geophysical Research Letters*. doi: 10.1002/2017GL073972.

Eyring, V. *et al.* (2016) 'Overview of the Coupled Model Intercomparison Project Phase 6 (CMIP6) experimental design and organization', *Geoscientific Model Development*. doi: 10.5194/gmd-9-1937-2016.

Gerlach, T. M., Westrich, H. R. and Symonds, R. B. (1996) 'Preeruption Vapor in Magma of the Climactic Mount Pinatubo Eruption: Source of the Giant Stratospheric Sulfur Dioxide Cloud', *Fire and Mud: Eruptions and lahars of Mount Pinatubo, Philippines*.

Ghan, S. J. (2013) 'Technical note: Estimating aerosol effects on cloud radiative forcing', *Atmospheric Chemistry and Physics*. doi: 10.5194/acp-13-9971-2013.

Guo, S. *et al.* (2004) 'Re-evaluation of SO2 release of the 15 June 1991 Pinatubo eruption using ultraviolet and infrared satellite sensors', *Geochemistry, Geophysics, Geosystems*. doi: 10.1029/2003GC000654.

Halmer, M. M., Schmincke, H. U. and Graf, H. F. (2002) 'The annual volcanic gas input into the atmosphere, in particular into the stratosphere: A global data set for the past 100 years', *Journal of Volcanology and Geothermal Research*. doi: 10.1016/S0377-0273(01)00318-3.

Hunton, D. E. *et al.* (2005) 'In-situ aircraft observations of the 2000 Mt. Hekla volcanic cloud: Composition and chemical evolution in the Arctic lower stratosphere', *Journal of Volcanology and Geothermal Research*. doi: 10.1016/j.jvolgeores.2005.01.005.

Iglesias-Suarez, F. *et al.* (2018) 'Key drivers of ozone change and its radiative forcing over the 21st century', *Atmospheric Chemistry and Physics*. doi: 10.5194/acp-18-6121-2018.

Kilian, M., Brinkop, S. and Jöckel, P. (2020) 'Impact of the eruption of Mt Pinatubo on the chemical composition of the stratosphere', *Atmospheric Chemistry and Physics*. doi: 10.5194/acp-20-11697-2020.

Kinne, S., Toon, O. B. and Prather, M. J. (1992) 'Buffering of stratospheric circulation by changing amounts of tropical ozone a Pinatubo Case Study', *Geophysical Research Letters*. doi: 10.1029/92GL01937.

Kremser, S. *et al.* (2016) 'Stratospheric aerosol - Observations, processes and impact on climate', *Reviews of Geophysics*. doi: 10.1002/2015RG000511.Received.

Krüger, K., Kutterolf, S. and Hansteen, T. H. (2015) 'Halogen release from Plinian eruptions and depletion of stratospheric ozone', in *Volcanism and Global Environmental Change*. doi: 10.1017/cbo9781107415683.020.

Kutterolf, S. *et al.* (2013) 'Combined bromine and chlorine release from large explosive volcanic eruptions: A

threat to stratospheric ozone?', *Geology*, 41(6), pp. 707–710. doi: 10.1130/G34044.1.

Kutterolf, S. *et al.* (2015) 'Bromine and chlorine emissions from Plinian eruptions along the Central American Volcanic Arc: From source to atmosphere', *Earth and Planetary Science Letters*. doi: 10.1016/j.epsl.2015.07.064.

Lacis, A. (2015) 'Volcanic aerosol radiative properties', *Science Highlights: Volcanoes and cCimate*.

Legrande, A. N., Tsigaridis, K. and Bauer, S. E. (2016) 'Role of atmospheric chemistry in the climate impacts of stratospheric volcanic injections', *Nature Geoscience*. doi: 10.1038/ngeo2771.

Loffler, M. (2015) *Impact of major volcanic eruptions on stratospheric water vapour*. Regensburg, Germany.

Löffler, M., Brinkop, S. and Jöckel, P. (2016) 'Impact of major volcanic eruptions on stratospheric water vapour', *Atmospheric Chemistry and Physics*. doi: 10.5194/acp-16-6547-2016.

Lurton, T. *et al.* (2018) 'Model simulations of the chemical and aerosol microphysical evolution of the Sarychev Peak 2009 eruption cloud compared to in situ and satellite observations', *Atmospheric Chemistry and Physics*. doi: 10.5194/acp-18-3223-2018.

Madronich, S. (2007) 'Analytic formula for the clear-sky UV index', *Photochemistry and Photobiology*. doi: 10.1111/j.1751-1097.2007.00200.x.

Mankin, W. G. and Coffey, M. T. (1984) 'Increased stratospheric hydrogen chloride in the El Chichon cloud.', *Science*. doi: 10.1126/science.226.4671.170.

Mankin, W. G., Coffey, M. T. and Goldman, A. (1992) 'Airborne observations of SO2, HCl, and O3 in the stratospheric plume of the Pinatubo Volcano in July 1991', *Geophysical Research Letters*. doi: 10.1029/91GL02942.

McCormick, M. P., Thomason, L. W. and Trepte, C. R. (1995) 'Atmospheric effects of the Mt Pinatubo eruption', *Nature*. doi: 10.1038/373399a0.

Mills, M. J. *et al.* (2016) 'Global volcanic aerosol properties derived from emissions, 1990–2014, using CESM1(WACCM)', *Journal of Geophysical Research*. doi: 10.1002/2015JD024290.

Ming, A. *et al.* (2020) 'Stratospheric Ozone Changes From Explosive Tropical Volcanoes: Modeling and Ice Core Constraints', *Journal of Geophysical Research: Atmospheres*. doi: 10.1029/2019JD032290.

Mulcahy, J. *et al.* (2020) 'Description and evaluation of aerosol in UKESM1 and HadGEM3-GC3.1 CMIP6 historical simulations', *Geoscientific Model Development Discussions*. doi: 10.5194/gmd-2019-357.

Newhall, C., Self, S. and Robock, A. (2018) 'Anticipating future Volcanic Explosivity Index (VEI) 7 eruptions and their chilling impacts', *Geosphere*. GeoScienceWorld, 14(2), pp. 572–603. doi: 10.1130/GES01513.1.

Osprey, S. M. *et al.* (2013) 'Stratospheric variability in twentieth-century CMIP5 simulations of the met office

climate model: High top versus low top', *Journal of Climate*. doi: 10.1175/JCLI-D-12-00147.1.

Prata, A. J. *et al.* (2007) 'Long range transport and fate of a stratospheric volcanic cloud from Soufrière Hills volcano, Montserrat', *Atmospheric Chemistry and Physics*. doi: 10.5194/acp-7-5093-2007.

Rap, A. *et al.* (2015) 'Satellite constraint on the tropospheric ozone radiative effect', *Geophysical Research Letters*. doi: 10.1002/2015GL064037.

Read, W., Froidvaux, L., Santee, M., and Livesey, N. (2009) 'Observations of volcanic SO2 and HCl from Aura MLS', in *Read, W., Froidvaux, L., Santee, M., and Livesey, N.: Observationsof volcanic SO2and HCl from Aura MLS, American Geophys-ical Union, Fall Meeting 2009, abstract number V24B-03, 14–18 December 2009.*

Robock, A. (2000) 'Volcanic eruptions and climate', *Reviews of Geophysics*. Wiley-Blackwell, 38(2), pp. 191–219. doi: 10.1029/1998RG000054.

Rose, W. I. *et al.* (2006) 'Atmospheric chemistry of a 33-34 hour old volcanic cloud from Hekla Volcano (Iceland): Insights from direct sampling and the application of chemical box modeling', *Journal of Geophysical Research Atmospheres*. doi: 10.1029/2005JD006872.

Schmidt, A. *et al.* (2018) 'Volcanic Radiative Forcing From 1979 to 2015', *Journal of Geophysical Research: Atmospheres*. doi: 10.1029/2018JD028776.

Self S, Zhao J-X, Holasek RE, Torres RC, K. A. (1996) 'The atmospheric impact of the 1991 Mount Pinatubo eruption.', in *Fire and Mud: Eruptions and lahars of Mount Pinatubo, Philippines*. Punongbaya. University of Washington Press.

Sellar, A. A. *et al.* (2019) 'UKESM1: Description and Evaluation of the U.K. Earth System Model', *Journal of Advances in Modeling Earth Systems*. doi: 10.1029/2019MS001739.

Sellar, A. A. *et al.* (2020) 'Implementation of U.K. Earth System Models for CMIP6', *Journal of Advances in Modeling Earth Systems*. doi: 10.1029/2019MS001946.

Solomon, S. *et al.* (1996) 'The role of aerosol variations in anthropogenic ozone depletion at northern midlatitudes', *JOURNAL OF GEOPHYSICAL RESEARCH*, 101(20), pp. 6713–6727. doi: 10.1029/95JD03353.

Solomon, S. (1999) 'Stratospheric ozone depletion: A review of concepts and history', *Reviews of Geophysics*. doi: 10.1029/1999RG900008.

Telford, P. J. *et al.* (2013) 'Implementation of the Fast-JX Photolysis scheme (v6.4) into the UKCA component of the MetUM chemistry-climate model (v7.3)', *Geoscientific Model Development*. doi: 10.5194/gmd-6-161-2013.

Textor, C. *et al.* (2003) 'Injection of gases into the stratosphere by explosive volcanic eruptions', *Journal of Geophysical Research: Atmospheres*. doi: 10.1029/2002jd002987.

Thomason, L. W. *et al.* (2018) 'A global space-based stratospheric aerosol climatology: 1979-2016', *Earth System Science Data*. doi: 10.5194/essd-10-469-2018.

Tie, X. X. and Brasseur, G. (1995) 'The response of stratospheric ozone to volcanic eruptions: Sensitivity to atmospheric chlorine loading', *Geophysical Research Letters*. doi: 10.1029/95GL03057.

Timmreck, C. *et al.* (2010) 'Aerosol size confines climate response to volcanic super-eruptions', *Geophysical Research Letters*. Wiley-Blackwell, 37(24), p. n/a-n/a. doi: 10.1029/2010GL045464.

Varekamp, J. C., Luhr, J. F. and Prestegaard, K. L. (1984) 'The 1982 eruptions of El Chichón Volcano (Chiapas, Mexico): Character of the eruptions, ash-fall deposits, and gasphase', *Journal of Volcanology and Geothermal Research*. doi: 10.1016/0377-0273(84)90056-8.

Vidal, C. M. *et al.* (2016) 'The 1257 Samalas eruption (Lombok, Indonesia): The single greatest stratospheric gas release of the Common Era', *Scientific Reports*. doi: 10.1038/srep34868.

Wade, D. C. *et al.* (2020) 'Reconciling the climate and ozone response to the 1257 CE Mount Samalas eruption', *Proceedings of the National Academy of Sciences of the United States of America*. doi: 10.1073/pnas.1919807117.

Wallace, L. and Livingston, W. (1992) 'The effect of the Pinatubo cloud on hydrogen chloride and hydrogen fluoride', *Geophysical Research Letters*. doi: 10.1029/92GL01112.

Woods, D. C., Chuan, R. L. and Rose, W. I. (1985) 'Halite particles injected into the stratosphere by the 1982 El Chichón eruption', *Science*. doi: 10.1126/science.230.4722.170.

World Health Organisation (1994) *Ultraviolet radiation : an authoritative scientific review of environmental and health effects of UV, with reference to global ozone layer depletion / published under the joint sponsorship of the United Nations Environment Programme, the International Com*.

World Meteorological Organization (WMO) (2014) *Scientific Assessment of Ozone Depletion: 2014*, *World Meteorological Organization, Global Ozone Research and Monitoring Project - Report No. 55*.

Zdanowicz, C. M., Zielinski, G. A. and Germani, M. S. (1999) 'Mount Mazama eruption: Calendrical age verified and atmospheric impact assessed', *Geology*. doi: 10.1130/0091-7613(1999)027<0621:MMECAV>2.3.CO;2.

Zhu, Y. *et al.* (2020) 'Persisting volcanic ash particles impact stratospheric SO2 lifetime and aerosol optical properties', *Nature Communications*. doi: 10.1038/s41467-020-18352-5.

Formatted: Space After: 12 pt